

An energy stable C^0 finite element scheme for a quasi-incompressible phase-field model of moving contact line with variable density



Lingyue Shen^a, Huaxiong Huang^{c,d,e}, Ping Lin^a, Zilong Song^{d,f}, Shixin Xu^{b,e,*}

^a Department of Mathematics, University of Dundee, Dundee DD1 4HN, Scotland, United Kingdom

^b Duke Kunshan University, 8 Duke Ave, Kunshan, Jiangsu, China

^c Joint Mathematical Research Centre of Beijing Normal University and BNU-HKBU United International College, Zhuhai, China

^d Department of Mathematics and Statistics, York University, Toronto, Ontario, Canada

^e Centre for Quantitative Analysis and Modelling, Fields Institute for Research in Mathematical Sciences, Toronto, Ontario, Canada

^f Department of Mathematics, University of California, Riverside, 900 University Avenue, Riverside, CA, USA

ARTICLE INFO

Article history:

Received 15 August 2019

Received in revised form 2 December 2019

Accepted 5 December 2019

Available online 10 December 2019

Keywords:

Energy stability

Moving contact lines

Large density ratio

Phase-field method

Quasi-incompressible

C^0 finite element

ABSTRACT

In this paper, we focus on modeling and simulation of two-phase flow problems with moving contact lines and variable density. A thermodynamically consistent phase-field model with general Navier boundary condition is developed based on the concept of quasi-incompressibility and the energy variational method. A mass conserving C^0 finite element scheme is proposed to solve the PDE system. Energy stability is achieved at the fully discrete level. Various numerical results confirm that the proposed scheme for both P^1 element and P^2 element are energy stable.

© 2019 Elsevier Inc. All rights reserved.

1. Introduction

The modeling and simulation of moving contact lines (MCLs), where the interface of two or more immiscible fluids intersects with a solid wall [1,2], have attracted much attention in recent years. Applications of MCLs in industries and medical fields (for example, printing [3], spray cooling of surfaces [4], blood clot [5], microfluidics [6], surfactant [7,8]) have motivated scientific interests and mathematical challenges on associated issues such as the stress singularity and contact angle hysteresis. In order to model the dynamics around the contact lines, various types of models and approximations have been developed, such as direct molecular dynamics simulations [9–11], phase-field models [12–19], microscopic–macroscopic hybrid model [20,21], front tracking model [22–24,8] and Lattice Boltzmann model [25,26]. For reviews of the current status of the MCLs problem, we refer to the articles [27] and [28].

Among those models, phase-field method (or diffusive interface method) [29–31] is one of the most popular and powerful methodologies. It has two main advantages. Firstly, it is easy to track the interface and numerically implement [32–34] even if there are topological changes [35]. Secondly, it can be derived by energy-based variational approach [36–38]. As a

* Corresponding author at: Duke Kunshan University, 8 Duke Ave, Kunshan, Jiangsu, China.

E-mail address: shixin.xu@dukekunshan.edu.cn (S. Xu).

result, the obtained system is compatible with the law of energy dissipation, which makes it possible to design efficient and energetically stable numerical schemes [39–42].

One of the main challenges in phase-field method is to model the immiscible two-phase flow with different densities. When the density ratio between the two phases is small, it could be handled by the Boussinesq approximation [43]. However, it could not be extended to the case with a large density ratio due to its underlying assumption [38]. One key problem arises from the inconsistency between the mass conservation and the incompressibility especially near the diffusive interface region. It was first pointed out by Lowengrub [44] and later by Shen et al. [38,45]. Two main approaches are proposed to overcome this difficulty: one is based on volume averaged velocity; the other is based on the mass averaged velocity. For the volume averaged velocity model, the incompressibility is assumed everywhere including the interfacial region [46–48,41,49]. A thermodynamically consistent and frame invariant model was developed by Abels et al. [50], where the mass conservation equation is modified with a mass correction term. On the other hand, for the mass averaged velocity method, the mass conservation is assured instead of incompressibility. This naturally yields the quasi-incompressible Navier-Stokes-Cahn-Hilliard (q-NSCH) model [44,51], which in fact leads to a slightly compressible mixture only inside the interfacial region.

In the present paper, we first rederive and generalize the thermodynamically consistent q-NSCH model in [44] from a variational point of view by combining with the Energy Variational Approach (EnVarA) [37,52,53] and Onsager's Variation Principle [8,23,24,50]. It starts from two functionals for the total energy and dissipation, together with the kinematic equations based on physical laws of conservation. The specific forms of the fluxes and stresses in the kinematic equations could be obtained by taking the time derivative of the total energetic functional and comparing with the predefined dissipation functional. More details could be found in [54]. In addition to bulk energy and dissipation, the energy and dissipation on the boundary are introduced to model the dynamics of contact lines. Our energy variational approach consistently yields both the correct bulk equations (the q-NSCH system) and a modified general Navier-Stokes Boundary condition (GNBC) for the case of mass averaged velocity. The density effect on the contact line is explicitly modeled compared with the traditional GNBC [14,15,55–58] in the case of volume averaged velocity, where the effect is modeled implicitly by the bulk and boundary interactions.

The second goal of our paper is to design an efficient energy stable scheme for the obtained q-NSCH system with large density ratio. There are not many such schemes developed for the MCLs. For the incompressible NSCH system, the development of such schemes may be found in [16,55,56,59–61,42,58] including higher order schemes [62–64] and only a few of them [56,58,61] are for variable density MCL models using the volume-averaged velocity (satisfying the incompressible condition in the whole domain). We shall develop an energy stable scheme for our thermodynamically consistent variable density q-NSCH system using the mass-averaged velocity. Based on the author's previous works [13,51,65], we design a mass conservative C^0 finite element method for the q-NSCH system with a consistent discrete energy law. Thanks to a Δp term in the quasi-incompressible condition, which is similar to the pressure stabilization of pseudo-compressibility methods [66–68], q-NSCH system does not need to satisfy the Babuska-Brezzi inf-sup condition [68–71]. This may be considered as another benefit of our quasi-incompressible NSCH system.

The rest of paper is organized as follows. In Section 2, we present the thermodynamically consistent derivation of the q-NSCH system and its non-dimensionalization. The C^0 finite element algorithm for the q-NSCH system and the energy stable analysis are shown in Section 3. Section 4 presents the numerical results, including the convergence case study, and the examples of moving droplets and rising bubbles.

2. Mathematical model

2.1. Mass-averaged velocity and laws of conservation

We consider a complex mixture consisting of two phase fluids with different densities. The interface of two fluids intersects with the wall $\partial\Omega_w$ at the contact line Γ_w (see Fig. 1 (a)). Around the interface, we choose a control volume $V(t)$, where there are two phases labeled by $i = 1, 2$ with volume V_i and mass M_i (see Fig. 1 (b)). If the local average density of each phase is denoted by $\bar{\rho}_i = M_i/V$ and pure phase density is denoted by $\rho_i = M_i/V_i$, then density of mixture is

$$\rho = \frac{M}{V} = \frac{M_1}{V} + \frac{M_2}{V} = \bar{\rho}_1 + \bar{\rho}_2. \quad (1)$$

Let $c_i = \frac{M_i}{M}$ be the mass fraction of each phase. Then we have [72]

$$\frac{1}{\rho} = \frac{V}{M} = \frac{V_1}{M} + \frac{V_2}{M} = \frac{c_1}{\rho_1} + \frac{c_2}{\rho_2} = \frac{c}{\rho_1} + \frac{1-c}{\rho_2}, \quad (2)$$

where $c = c_1$ is adopted in the last equality.

Remark 2.1. Note that according to the definition (2), the mixture density ρ is almost constant everywhere except in the interfacial region.

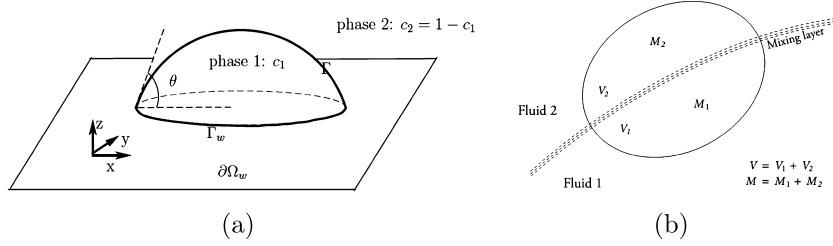


Fig. 1. Schematic of moving contact line problems (a) and interface (b).

If we assume those two fluids move with velocities \mathbf{u}_i ($i = 1, 2$), then the mass conservation of each phase inside the control volume is

$$\frac{\partial \bar{\rho}_i}{\partial t} + \nabla \cdot (\mathbf{u}_i \bar{\rho}_i) = 0, \quad i = 1, 2. \quad (3)$$

Introducing the mass averaged velocity as

$$\rho \mathbf{u} = \bar{\rho}_1 \mathbf{u}_1 + \bar{\rho}_2 \mathbf{u}_2, \quad (4)$$

and combining with Eq. (1) yields the conservation of mass for the mixture

$$\frac{\partial \rho}{\partial t} + \nabla \cdot (\rho \mathbf{u}) = 0. \quad (5)$$

Next, with an arbitrary volume $V(t) \in \Omega$, laws of conservation state

$$\frac{d}{dt} \int_{V(t)} \rho c dx = - \int_{\partial V(t)} \mathbf{j}_c \cdot \mathbf{n} dS, \quad (6)$$

$$\frac{d}{dt} \int_{V(t)} \rho \mathbf{u} dx = \int_{\partial V(t)} (\boldsymbol{\sigma}_\eta + \boldsymbol{\sigma}_c) \cdot \mathbf{n} dS. \quad (7)$$

Here, the first equation is the conservation of phase-field function (phase 1) and \mathbf{j}_c is the flux of phase-field function. The second equation is the conservation of momentum where $\boldsymbol{\sigma}_\eta$ is the viscous stress and $\boldsymbol{\sigma}_c$ is the extra stress induced by two-phase interface due to nonzero ∇c .

Thanks to the Reynolds transport theory [51,54], Eqs. (5)-(7) yield the following kinematic equations in the domain Ω

$$\begin{cases} \rho \frac{Dc}{Dt} = -\nabla \cdot \mathbf{j}_c, \\ \frac{D\rho}{dt} + \rho \nabla \cdot \mathbf{u} = \frac{\partial \rho}{\partial t} + \nabla \cdot (\rho \mathbf{u}) = 0, \\ \rho \frac{D\mathbf{u}}{Dt} = \nabla \cdot \boldsymbol{\sigma}_\eta + \nabla \cdot \boldsymbol{\sigma}_c, \end{cases} \quad (8)$$

where $\frac{D}{Dt} = \frac{\partial}{\partial t} + \mathbf{u} \cdot \nabla$ is the material derivative.

By definition of $\rho = \rho(c(\mathbf{x}, t))$ in Eq. (2), above equations yield the quasi-incompressibility condition [44,51]

$$\nabla \cdot \mathbf{u} = -\frac{1}{\rho} \frac{D\rho}{Dt} = \frac{1}{\rho^2} \frac{d\rho}{dc} (\nabla \cdot \mathbf{j}_c). \quad (9)$$

In the present case, we denote

$$\alpha = -\frac{1}{\rho^2} \frac{d\rho}{dc} = \frac{\rho_2 - \rho_1}{\rho_1 \rho_2}, \quad (10)$$

then the quasi-incompressibility condition is written as

$$\nabla \cdot \mathbf{u} = -\alpha \nabla \cdot \mathbf{j}_c. \quad (11)$$

Remark 2.2. Equations (10)-(11) show that the quasi-incompressibility condition depends on the density difference of two fluids. When the two phases have the same density, i.e. $\rho_1 = \rho_2$, it will consistently degenerate to the incompressibility condition. It makes a difference when two fluids have large density ratio and near the interfacial region [44,51,72].

On the boundary of domain $\partial\Omega$, the following boundary conditions are used

$$\begin{cases} \mathbf{u} \cdot \mathbf{n} = 0, & \mathbf{u}^s \cdot \boldsymbol{\tau}_i = u_{\tau_i}^s = f_{\tau_i} \\ \frac{D_{\Gamma}c}{Dt} = J_{\Gamma}, \\ \mathbf{j}_c \cdot \mathbf{n} = 0, \end{cases} \quad (12)$$

where $\mathbf{u}^s = \mathbf{u}_{\tau} - \mathbf{u}_w$ with $\mathbf{u}_{\tau} = \mathbf{u} - (\mathbf{u} \cdot \mathbf{n})\mathbf{n}$ is the fluid slip velocity with respect to the wall, $\frac{D_{\Gamma}c}{Dt} = \frac{\partial c}{\partial t} + \mathbf{u} \cdot \nabla_{\Gamma}c$ is the surface material derivative, the Allen-Cahn type boundary condition is used for c and $\nabla_{\Gamma} = \nabla - \mathbf{n}(\mathbf{n} \cdot \nabla)$ is surface gradient on the boundary $\partial\Omega$. The quantities f_{τ_i} and J_{Γ} are to be determined. During the derivation, we assume the solid wall is fixed, i.e. $\mathbf{u}^s = \mathbf{u}_{\tau}$.

2.2. Model derivation

Now we start to derive the exact forms of \mathbf{j}_c , $\boldsymbol{\sigma}_{\eta}$, $\boldsymbol{\sigma}_c$ in Eq. (8), f_{τ_i} and J_{Γ} in Eq. (12) by using energy variational method.

The total energy consists of the kinetic energy, the phase mixing energy and the energy on solid wall boundary $\partial\Omega_w$

$$\begin{aligned} E^{tot} &= E_{kin} + E_{mix} + E_w \\ &= \int_{\Omega} \frac{\rho(c)|\mathbf{u}|^2}{2} d\mathbf{x} + \int_{\Omega} \lambda_c \rho(c) \left(G(c) + \frac{\gamma^2}{2} |\nabla c|^2 \right) d\mathbf{x} + \int_{\partial\Omega_w} f_w(c) dS, \end{aligned} \quad (13)$$

together with

$$G(c) = \frac{1}{4}c^2(1-c)^2, \quad f_w(c) = -\frac{\sigma}{2} \cos(\theta_s) \sin\left(\frac{(2c-1)\pi}{2}\right), \quad (14)$$

where λ_c is the mixing energy density, γ is the capillary width of the interface, θ_s is static contact angle and σ is surface tension. The mixing energy E_{mix} represents the competition between a homogeneous bulk mixing energy density term $G(c)$ ('hydrophobic' part) that enforces total separation of the two phases into pure components, and a gradient distortional term $\frac{|\nabla c|^2}{2}$ ('hydrophilic' part) that represents the nonlocal interactions between two phases and penalizes spatial heterogeneity.

The dissipation functional is composed of the dissipation due to fluid friction and irreversible mixing of two phases in bulk and the dissipation on the boundary

$$\Delta = \int_{\Omega} 2\eta(c)|\mathbf{D}_{\eta}|^2 d\mathbf{x} + \int_{\Omega} \lambda(c)|\nabla \cdot \mathbf{u}|^2 d\mathbf{x} + \int_{\Omega} \frac{1}{\mathcal{M}} |\mathbf{j}_c|^2 d\mathbf{x} + \int_{\partial\Omega_w} \left(\frac{1}{\mathcal{M}_{\Gamma}} J_{\Gamma}^2 + \beta_{\Gamma} |\mathbf{u}^s|^2 \right) dS, \quad (15)$$

where $\lambda(c)$ and $\eta(c)$ are the two Lamé coefficients, $\mathbf{D}_{\eta} = (\nabla \mathbf{u} + (\nabla \mathbf{u})^T)/2$ is the strain rate, \mathcal{M} is mobility coefficient in bulk, \mathcal{M}_{Γ} is mobility coefficient on the wall, $\beta_{\Gamma}(c)$ is wall friction coefficient. In the present paper, $\eta(c)$ and β_{Γ} are approximated by

$$\frac{1}{\eta(c)} = \frac{c}{\eta_1} + \frac{(1-c)}{\eta_2}, \quad \frac{1}{\beta_{\Gamma}(c)} = \frac{c}{\beta_{\Gamma_1}} + \frac{(1-c)}{\beta_{\Gamma_2}},$$

where η_i and β_{Γ_i} with $i = 1, 2$ are coefficients of each phase.

During the derivation, the following lemma is frequently used.

Lemma 2.1. For a continuous function $f(\mathbf{x}, t)$, if the density ρ satisfies the conservation law (5) in the domain Ω and $\mathbf{u} \cdot \mathbf{n} = 0$ on the boundary $\partial\Omega$, then we have

$$\frac{d}{dt} \int_{\Omega} \rho(\mathbf{x}, t) f(\mathbf{x}, t) d\mathbf{x} = \int_{\Omega} \rho \frac{Df}{Dt} d\mathbf{x}.$$

By taking the time derivative of the total energetic functional, we have

$$\frac{dE^{tot}}{dt} = \frac{d}{dt} E_{kin} + \frac{d}{dt} E_{mix} + \frac{d}{dt} E_w = I_1 + I_2 + I_3. \quad (16)$$

For the first term in (16), using the last two equations in Eq. (8) yields

$$\begin{aligned}
I_1 &= \frac{d}{dt} \int_{\Omega} \frac{\rho |\mathbf{u}|^2}{2} d\mathbf{x} \\
&= - \int_{\Omega} (\boldsymbol{\sigma}_{\eta} : \nabla \mathbf{u} + \boldsymbol{\sigma}_c : \nabla \mathbf{u}) d\mathbf{x} + \int_{\Omega} \alpha \nabla p \cdot \mathbf{j}_c d\mathbf{x} - \int_{\Omega} p \nabla \cdot \mathbf{u} d\mathbf{x} \\
&\quad + \int_{\partial\Omega_w} ((\boldsymbol{\sigma}_{\eta} + \boldsymbol{\sigma}_c) \cdot \mathbf{n}) \cdot \mathbf{u}_{\tau} dS,
\end{aligned} \tag{17}$$

where we have introduced a Lagrangian multiplier p with respect to the quasi-compressibility condition (9) and have used the boundary conditions $\mathbf{u} \cdot \mathbf{n} = 0$ and $\mathbf{j}_c \cdot \mathbf{n} = 0$. For the second term in (16), using the first equation in Eq. (8) and last two boundary conditions in Eq. (12) yields

$$\begin{aligned}
I_2 &= \frac{d}{dt} \int_{\Omega} \rho \lambda_c \left(G(c) + \frac{\gamma^2}{2} |\nabla c|^2 \right) d\mathbf{x} \\
&= \int_{\Omega} \nabla \mu \cdot \mathbf{j}_c d\mathbf{x} - \int_{\Omega} \lambda_c \gamma^2 (\rho \nabla c \otimes \nabla c) : \nabla \mathbf{u} d\mathbf{x} + \int_{\partial\Omega_w} \rho \lambda_c \gamma^2 \partial_n c \frac{D_{\Gamma} c}{Dt} dS,
\end{aligned} \tag{18}$$

where $\mu = \lambda_c \left(\frac{dG}{dc} - \frac{1}{\rho} \gamma^2 \nabla \cdot (\rho \nabla c) \right)$. The detailed derivations of Eqs. (17)-(18) are given in Appendix A. The last term I_3 in (16) yields

$$I_3 = \frac{d}{dt} \int_{\partial\Omega_w} f_w dS = \int_{\partial\Omega_w} \frac{df_w}{dc} \frac{\partial c}{\partial t} dS. \tag{19}$$

Combining Eqs. (17)-(19), we obtain the derivative of the energy functional

$$\begin{aligned}
\frac{dE^{tot}}{dt} &= - \int_{\Omega} \boldsymbol{\sigma}_{\eta} : \nabla \mathbf{u} d\mathbf{x} - \int_{\Omega} (\boldsymbol{\sigma}_c + \lambda_c \gamma^2 \rho \nabla c \otimes \nabla c) : \nabla \mathbf{u} d\mathbf{x} \\
&\quad + \int_{\Omega} \nabla \mu \cdot \mathbf{j}_c d\mathbf{x} + \int_{\Omega} \nabla(\alpha p) \cdot \mathbf{j}_c d\mathbf{x} - \int_{\Omega} p \nabla \cdot \mathbf{u} d\mathbf{x} \\
&\quad + \int_{\partial\Omega_w} ((\boldsymbol{\sigma}_{\eta} + \boldsymbol{\sigma}_c) \cdot \mathbf{n}) \cdot \mathbf{u}_{\tau} dS + \int_{\partial\Omega_w} \rho \lambda_c \gamma^2 \partial_n c \frac{D_{\Gamma} c}{Dt} dS + \int_{\partial\Omega_w} \frac{df_w}{dc} \frac{\partial c}{\partial t} dS \\
&= - \int_{\Omega} \boldsymbol{\sigma}_{\eta} : \nabla \mathbf{u} d\mathbf{x} - \int_{\Omega} (\boldsymbol{\sigma}_c + \lambda_c \gamma^2 \rho \nabla c \otimes \nabla c) : \nabla \mathbf{u} d\mathbf{x} \\
&\quad + \int_{\Omega} \nabla \tilde{\mu} \cdot \mathbf{j}_c d\mathbf{x} - \int_{\Omega} p \nabla \cdot \mathbf{u} d\mathbf{x} \\
&\quad + \int_{\partial\Omega_w} \left((\boldsymbol{\sigma}_{\eta} + \boldsymbol{\sigma}_c) \cdot \mathbf{n} - \frac{df_w}{dc} \nabla_{\Gamma} c \right) \cdot \mathbf{u}_{\tau} dS + \int_{\partial\Omega_w} L(c) \frac{D_{\Gamma} c}{Dt} dS \\
&= - \int_{\Omega} \boldsymbol{\sigma}_{\eta} : \nabla \mathbf{u} d\mathbf{x} - \int_{\Omega} (\boldsymbol{\sigma}_c + \lambda_c \gamma^2 \rho \nabla c \otimes \nabla c) : \nabla \mathbf{u} d\mathbf{x} \\
&\quad + \int_{\Omega} \nabla \tilde{\mu} \cdot \mathbf{j}_c d\mathbf{x} - \int_{\Omega} p \nabla \cdot \mathbf{u} d\mathbf{x} \\
&\quad + \int_{\partial\Omega_w} \left((\boldsymbol{\sigma}_{\eta} + \boldsymbol{\sigma}_c) \cdot \mathbf{n} - \frac{df_w}{dc} \nabla_{\Gamma} c \right) \cdot \mathbf{u}_{\tau} dS + \int_{\partial\Omega_w} L(c) J_{\Gamma} dS,
\end{aligned} \tag{20}$$

where we have defined

$$\tilde{\mu} = \mu + \alpha p = \lambda_c \frac{dG}{dc} - \frac{\lambda_c \gamma^2}{\rho} \nabla \cdot (\rho \nabla c) + \alpha p, \quad (21)$$

$$L(c) = \rho \lambda_c \gamma^2 \partial_n c + \frac{df_w}{dc}. \quad (22)$$

Using energy dissipation law $dE^{tot}/dt = -\Delta$ [52,73] and comparing (20) with the predefined dissipation functional in Eq. (15) yield

$$\begin{cases} \mathbf{j}_c = -\mathcal{M} \nabla \tilde{\mu}, \\ \boldsymbol{\sigma}_\eta = 2\eta \mathbf{D}_\eta + \lambda \nabla \cdot \mathbf{u} \mathbf{I} - p \mathbf{I} = \eta (\nabla \mathbf{u} + (\nabla \mathbf{u})^T) + \lambda \nabla \cdot \mathbf{u} \mathbf{I} - p \mathbf{I}, \\ \boldsymbol{\sigma}_c = -\lambda_c \gamma^2 \rho (\nabla c \otimes \nabla c), \\ J_\Gamma = -\mathcal{M}_\Gamma L(c), \\ u_{\tau_i}^s = \beta_\Gamma^{-1} \boldsymbol{\tau}_i \cdot (-\boldsymbol{\sigma}_\eta + \boldsymbol{\sigma}_c) \cdot \mathbf{n} + \frac{df_w}{dc} \nabla_\Gamma c. \end{cases} \quad (23)$$

By the definition of $\boldsymbol{\sigma}_\eta$ and $\boldsymbol{\sigma}_c$, the slip boundary condition (last equation in (23)) could be further written in the GNBC format

$$u_{\tau_i}^s = \beta_\Gamma^{-1} \boldsymbol{\tau}_i \cdot (-\boldsymbol{\sigma}_\eta \cdot \mathbf{n} + L(c) \nabla_\Gamma c). \quad (24)$$

To summarize, we have the following model for the two-phase flow with variable density for three unknowns c, \mathbf{u}, p , in domain Ω ,

$$\rho \frac{Dc}{Dt} = \nabla \cdot (\mathcal{M} \nabla \tilde{\mu}), \quad (25a)$$

$$\tilde{\mu} = \lambda_c \frac{dG}{dc} - \frac{\lambda_c \gamma^2}{\rho} \nabla \cdot (\rho \nabla c) + \alpha p, \quad (25b)$$

$$\frac{D\rho}{Dt} + \rho \nabla \cdot \mathbf{u} = 0, \quad (25c)$$

$$\rho \frac{D\mathbf{u}}{Dt} = \nabla \cdot (2\eta \mathbf{D}_\eta) + \nabla (\lambda \nabla \cdot \mathbf{u}) - \nabla p - \nabla \cdot (\lambda_c \gamma^2 \rho \nabla c \otimes \nabla c), \quad (25d)$$

with boundary conditions on $\partial\Omega$

$$\begin{cases} \frac{D_\Gamma c}{Dt} = -\mathcal{M}_\Gamma L(c), \\ \nabla \tilde{\mu} \cdot \mathbf{n} = 0, \\ \mathbf{u} \cdot \mathbf{n} = 0, \\ u_{\tau_i}^s = \beta_\Gamma^{-1} (-\mathbf{n} \cdot \boldsymbol{\sigma}_\eta \cdot \boldsymbol{\tau}_i) + L(c) \partial_{\tau_i} c, i = 1, 2, \end{cases} \quad (26)$$

where $L(c)$ and $\boldsymbol{\sigma}_\eta$ are defined in (22) and (23).

Remark 2.3. Note that in the above boundary conditions (26), the density effect on the contact line dynamics is explicitly modeled both in the boundary dynamics of phase-field and in velocity slip boundary condition through $L(c)$ term.

It is worth noting that the above system satisfies the following energy dissipation law.

Theorem 2.2. If c, \mathbf{u}, p are smooth solutions of above system (25)-(26), then the following energy law is satisfied:

$$\begin{aligned} \frac{dE^{tot}}{dt} &= \frac{d}{dt} \left\{ \int_\Omega \frac{\rho |\mathbf{u}|^2}{2} d\mathbf{x} + \int_\Omega \lambda_c \rho \left(G(c) + \frac{\gamma^2}{2} |\nabla c|^2 \right) d\mathbf{x} + \int_{\partial\Omega_w} f_w(c) dS \right\} \\ &= - \int_\Omega 2\eta |\mathbf{D}_\eta|^2 d\mathbf{x} - \int_\Omega \lambda |\nabla \cdot \mathbf{u}|^2 d\mathbf{x} - \int_\Omega \mathcal{M} |\nabla \tilde{\mu}|^2 d\mathbf{x} \\ &\quad - \int_{\partial\Omega_w} (\mathcal{M}_\Gamma |L(c)|^2 + \beta_\Gamma |\mathbf{u}^s|^2) dS. \end{aligned} \quad (27)$$

Proof. The main idea of the proof is obtained by multiplying the phase-field equation (25a) by $\tilde{\mu}$, multiplying the chemical potential equation (25b) by $\frac{dc}{dt}$, multiplying the mass conservation equation (25c) by p , multiplying the Navier-Stokes equation (25d) by \mathbf{u} , and summing them up.

Taking the inner product of the phase-field equation (25a) with $\tilde{\mu}$ results in the following equation

$$\int_{\Omega} \rho \frac{Dc}{Dt} \tilde{\mu} d\mathbf{x} = - \int_{\Omega} \mathcal{M} |\nabla \tilde{\mu}|^2 d\mathbf{x}, \tag{28}$$

where we used the boundary condition $\partial_n \tilde{\mu} = 0$ in (26).

Multiplying the chemical potential (25b) by $\rho \frac{Dc}{Dt}$ yields

$$\int_{\Omega} \tilde{\mu} \rho \frac{Dc}{Dt} = \int_{\Omega} \lambda_c \rho \frac{DG}{Dt} d\mathbf{x} + \int_{\Omega} \lambda \gamma^2 \nabla c \nabla \left(\frac{Dc}{Dt} \right) d\mathbf{x} - \int_{\Omega} \frac{p}{\rho} \frac{d\rho}{dc} \frac{Dc}{Dt} d\mathbf{x} - \int_{\partial\Omega_w} \lambda \gamma^2 \rho \partial_n c \frac{Dc}{Dt} dS. \tag{29}$$

Summing up the above two equations, we have

$$\begin{aligned} & \int_{\Omega} \lambda_c \rho \frac{DG}{Dt} d\mathbf{x} + \int_{\Omega} \lambda \gamma^2 \nabla c \nabla \left(\frac{Dc}{Dt} \right) d\mathbf{x} \\ &= - \int_{\Omega} \mathcal{M} |\nabla \tilde{\mu}|^2 d\mathbf{x} + \int_{\Omega} \frac{p}{\rho} \frac{d\rho}{dc} \frac{Dc}{Dt} d\mathbf{x} + \int_{\partial\Omega_w} \lambda \gamma^2 \rho \partial_n c \frac{Dc}{Dt} dS. \end{aligned} \tag{30}$$

Multiplying the Navier-stokes equation (25d) by \mathbf{u} followed by integration by parts, the rate of change of kinetic energy is calculated as

$$\begin{aligned} & \frac{d}{dt} \int_{\Omega} \rho \frac{|\mathbf{u}|^2}{2} d\mathbf{x} \\ &= - \int_{\Omega} 2\eta |\mathbf{D}\eta|^2 d\mathbf{x} - \int_{\Omega} \lambda |\nabla \cdot \mathbf{u}|^2 d\mathbf{x} + \int_{\Omega} p \nabla \cdot \mathbf{u} d\mathbf{x} + \int_{\Omega} \lambda \gamma^2 \rho (\nabla c \otimes \nabla c) : \nabla \mathbf{u} d\mathbf{x} \\ & \quad - \int_{\partial\Omega_w} \beta_{\Gamma} |\mathbf{u}^s|^2 + \int_{\partial\Omega_w} \frac{df_w}{dc} \nabla_{\Gamma} c \cdot \mathbf{u}_{\tau} dS \\ &= - \int_{\Omega} 2\eta |\mathbf{D}\eta|^2 d\mathbf{x} - \int_{\Omega} \lambda |\nabla \cdot \mathbf{u}|^2 d\mathbf{x} + \int_{\Omega} p \nabla \cdot \mathbf{u} d\mathbf{x} + \int_{\Omega} \lambda \gamma^2 \rho (\nabla c \otimes \nabla c) : \nabla \mathbf{u} d\mathbf{x} \\ & \quad - \int_{\partial\Omega_w} \beta_{\Gamma} |\mathbf{u}^s|^2 - \frac{d}{dt} \int_{\partial\Omega_w} f_w dS - \int_{\partial\Omega_w} \frac{df_w}{dc} \mathcal{M}_{\Gamma} L(c) dS, \end{aligned} \tag{31}$$

where we have used the definition $\frac{D_{\Gamma}c}{Dt} = \frac{\partial c}{\partial t} + \mathbf{u}_{\tau} \cdot \nabla_{\Gamma} c$, $\mathbf{u}_{\tau} = \mathbf{u}^s$ and boundary conditions in (26).

From the derivation of I_2 in Appendix A, we get

$$\begin{aligned} & \frac{d}{dt} \int_{\Omega} \rho \lambda_c \left(G(c) + \frac{\gamma^2}{2} |\nabla c|^2 \right) d\mathbf{x} \\ &= \int_{\Omega} \rho \lambda_c \frac{DG}{Dt} d\mathbf{x} + \int_{\Omega} \rho \lambda_c \gamma^2 \nabla c \cdot \nabla \left(\frac{Dc}{Dt} \right) d\mathbf{x} - \int_{\Omega} \rho \lambda_c \gamma^2 (\nabla c \otimes \nabla c) : \nabla \mathbf{u} d\mathbf{x}. \end{aligned} \tag{32}$$

Combining the equations (30)-(32) leads to the final energy dissipation law. \square

Remark 2.4. In the above derivation, we have neglected the external body force, for example the gravity. If the effect of gravity needs to be taken into consideration, an extra gravitational potential should be added to the total energy

$$E^{tot} = \int_{\Omega} \frac{\rho |\mathbf{u}|^2}{2} d\mathbf{x} + \int_{\Omega} \lambda_c \rho \left(G(c) + \frac{\gamma^2}{2} |\nabla c|^2 \right) d\mathbf{x} + \int_{\partial\Omega_w} f_w(c) dS + \int_{\Omega} \rho g z d\mathbf{x}, \tag{33}$$

where g is the gravitational constant and z is the vertical position. Using the fact that [72]

$$\frac{d}{dt} \int_{\Omega} \rho g z d v = \int_{\Omega} \rho g \mathbf{u} \cdot \mathbf{e}_z d \mathbf{x}, \quad \mathbf{e}_z = (0, 0, 1)^T, \quad (34)$$

the conservation of momentum equation (25d) is changed to

$$\rho \frac{D \mathbf{u}}{D t} = \nabla \cdot (2 \eta \mathbf{D} \eta) + \nabla (\lambda \nabla \cdot \mathbf{u}) - \nabla p - \nabla \cdot (\lambda_c \gamma^2 \rho \nabla c \otimes \nabla c) - \rho g \mathbf{e}_z. \quad (35)$$

2.3. Non-dimensionalization and reformulation

In the following parts of the article, we assume that $\lambda = -\frac{2\eta}{3}$ for simplicity. Now we introduce the dimensionless variables

$$\begin{aligned} \hat{x} &= \frac{x}{L^*}, & \hat{\mathbf{u}} &= \frac{\mathbf{u}}{U^*}, & \hat{\rho} &= \frac{\rho}{\rho^*}, & \hat{t} &= \frac{t}{t^*}, & \hat{\mu} &= \frac{\tilde{\mu}}{\mu^*}, & \hat{p} &= \frac{p}{P^*}, \\ \hat{\eta} &= \frac{\eta}{\eta^*}, & M &= \frac{\mathcal{M}}{\mathcal{M}^*}, & M_{\Gamma} &= \frac{\mathcal{M}_{\Gamma}}{\mathcal{M}_{\Gamma}^*}, & l_s^{-1} &= \frac{\beta_{\Gamma}}{\beta_{\Gamma}^*}, & \epsilon &= \frac{\gamma}{L^*}. \end{aligned} \quad (36)$$

Here L^* , U^* , ρ^* , η^* and \mathcal{M}^* are the characteristic scales of length, velocity, density, viscosity, and mobility coefficient, which are defined as

$$t^* = \frac{L^*}{U^*}, \quad \mu^* = \lambda_c \epsilon, \quad P^* = \rho^* \mu^*, \quad \mathcal{M}^* = \frac{\rho^* U^* L^*}{\mu^*}, \quad \mathcal{M}_{\Gamma}^* = \frac{1}{t^* \rho^* \lambda_c \gamma}, \quad \beta_{\Gamma}^* = \frac{\eta^*}{L^*}. \quad (37)$$

For convenience, the hat symbol will be removed in the dimensionless quantities, and the dimensionless system of (25,26) is given by

$$\rho \frac{D c}{D t} = \nabla \cdot (M \nabla \tilde{\mu}), \quad (38a)$$

$$\tilde{\mu} = \frac{1}{\epsilon} \frac{d G}{d c} - \frac{\epsilon}{\rho} \nabla \cdot (\rho \nabla c) + \alpha p, \quad (38b)$$

$$R e \rho \frac{D \mathbf{u}}{D t} = \nabla \cdot (\eta (\nabla \mathbf{u} + (\nabla \mathbf{u})^T)) - \nabla \left(\frac{2 \eta}{3} \nabla \cdot \mathbf{u} \right) - \frac{R e}{\beta} \nabla p - \frac{R e}{\beta} \epsilon \nabla \cdot (\rho \nabla c \otimes \nabla c), \quad (38c)$$

$$\nabla \cdot \mathbf{u} = \alpha \nabla \cdot (M \nabla \tilde{\mu}), \quad (38d)$$

with boundary conditions

$$\frac{D_{\Gamma} c}{D t} = -M_{\Gamma} L(c), \quad (39a)$$

$$\partial_n \tilde{\mu} = 0, \quad (39b)$$

$$\mathbf{u} \cdot \mathbf{n} = 0, \quad (39c)$$

$$l_s^{-1} u_{\tau_i}^s = -\mathbf{n} \cdot \boldsymbol{\sigma}_{\eta} \cdot \boldsymbol{\tau}_i + \frac{R e}{\beta} L \partial_{\tau_i} c, \quad (39d)$$

where

$$L(c) = \epsilon \rho \partial_n c + \alpha_w \frac{d f_w}{d c}, \quad f_w(c) = -\frac{1}{2} \cos(\theta_s) \sin\left(\frac{(2c-1)\pi}{2}\right), \quad (40)$$

and with dimensionless parameters

$$R e = \frac{\rho^* U^* L^*}{\eta^*}, \quad \beta = \frac{(U^*)^2}{\mu^*}, \quad \alpha_w = \frac{\sigma}{\rho^* \lambda_c \gamma}. \quad (41)$$

If we define

$$\bar{p} = p + \rho \left(\frac{1}{\epsilon} G(c) + \frac{\epsilon}{2} |\nabla c|^2 \right), \quad (42a)$$

$$\bar{\mu} = \tilde{\mu} - \alpha \bar{p}, \quad (42b)$$

then the system (38) could be rewritten as

$$\rho \frac{Dc}{Dt} = \nabla \cdot (M \nabla \bar{\mu}) + \alpha \nabla \cdot (M \nabla \bar{p}), \tag{43a}$$

$$\bar{\mu} = \frac{1}{\epsilon} \frac{dG}{dc} - \frac{\epsilon}{\rho} \nabla \cdot (\rho \nabla c) - \alpha \rho \left(\frac{1}{\epsilon} G(c) + \frac{\epsilon}{2} |\nabla c|^2 \right), \tag{43b}$$

$$Re \rho \frac{D\mathbf{u}}{Dt} = \nabla \cdot (\eta (\nabla \mathbf{u} + (\nabla \mathbf{u})^T)) - \nabla \cdot \left(\frac{2\eta}{3} \nabla \cdot \mathbf{u} \right) - \frac{Re}{\beta} \nabla \bar{p} + \frac{Re}{\beta} \rho \bar{\mu} \nabla c \tag{43c}$$

$$\nabla \cdot \mathbf{u} = \alpha \nabla \cdot (M \nabla \bar{\mu}) + \alpha^2 \nabla \cdot (M \nabla \bar{p}). \tag{43d}$$

If we define the Sobolev spaces as follows

$$\mathbf{W}^{1,3}(\Omega) = (W^{1,3}(\Omega))^2, \tag{44}$$

$$\mathbf{W}_b^{1,3}(\Omega) = \{\mathbf{u} = (u_x, u_y)^T \in \mathbf{W}^{1,3} | u_y = b, \text{ on } \partial\Omega_w\}, \tag{45}$$

$$\mathbf{W}_b = W^{1,3}(\Omega) \times W^{1,3}(\Omega) \times \mathbf{W}_b^{1,3}(\Omega) \times W^{1,3/2}(\Omega), \tag{46}$$

and then above system satisfies the following energy dissipation law.

Theorem 2.3. *If $(c, \mu, \mathbf{u}, \bar{p}) \in \mathbf{W}_b$, are smooth solutions of above system (43) with boundary conditions (39), then the following energy law is satisfied:*

$$\begin{aligned} \frac{d\mathcal{E}^{tot}}{dt} &= \frac{d}{dt} \left\{ \int_{\Omega} \frac{\rho |\mathbf{u}|^2}{2} d\mathbf{x} + \frac{1}{\beta} \int_{\Omega} \rho \left(\frac{1}{\epsilon} G(c) + \frac{\epsilon}{2} |\nabla c|^2 \right) d\mathbf{x} + \frac{\alpha_w}{\beta} \int_{\partial\Omega_w} f_w dS \right\} \\ &= -\frac{1}{Re} \int_{\Omega} \eta \sum_{i<j} |\partial_i u_j + \partial_j u_i|^2 d\mathbf{x} - \frac{2}{3Re} \int_{\Omega} \eta \sum_{i<j} |\partial_i u_i - \partial_j u_j|^2 d\mathbf{x} - \frac{1}{\beta} \int_{\Omega} M^n |\nabla \bar{\mu}|^2 d\mathbf{x} \\ &\quad - \int_{\partial\Omega_w} \left(\frac{1}{\beta} M_{\Gamma} |L(c)|^2 + \frac{1}{l_s Re} |\mathbf{u}^s|^2 \right) dS. \end{aligned} \tag{47}$$

The proof is similar as Theorem 2.2. Here we omit the details.

Remark 2.5. When the walls move, i.e. $\mathbf{u}_w \neq 0$, the above energy dissipation law has an extra term induced by external energy input

$$\begin{aligned} \frac{d\mathcal{E}^{tot}}{dt} &= -\frac{1}{Re} \int_{\Omega} \eta \sum_{i<j} |\partial_i u_j + \partial_j u_i|^2 d\mathbf{x} - \frac{2}{3Re} \int_{\Omega} \eta \sum_{i<j} |\partial_i u_i - \partial_j u_j|^2 d\mathbf{x} - \frac{1}{\beta} \int_{\Omega} M^n |\nabla \bar{\mu}|^2 d\mathbf{x} \\ &\quad - \int_{\partial\Omega_w} \left(\frac{1}{\beta} M_{\Gamma} |L(c)|^2 + \frac{1}{l_s Re} |\mathbf{u}^s|^2 \right) dS - \int_{\partial\Omega_w} \frac{1}{l_s Re} \mathbf{u}^s \cdot \mathbf{u}_w dS. \end{aligned} \tag{48}$$

3. Numerical scheme and analysis

3.1. Time-discrete primitive method

In this section, we present the numerical method of system (43) with boundary conditions (39) in the primitive variable formulation. Let $\Delta t > 0$ denote the time step, and assume $(c^n, \bar{\mu}^n, \mathbf{u}^n, \bar{p}^n)$ are the solutions at the time $t = n\Delta t$. We then find the solutions at time $t = (n + 1)\Delta t$ are $(c^{n+1}, \bar{\mu}^{n+1}, \mathbf{u}^{n+1}, \bar{p}^{n+1})$ that satisfy

$$\rho^n \frac{c^{n+1} - c^n}{\Delta t} + \rho^{n+1} (\mathbf{u}^{n+1} \cdot \nabla) c^{n+1} = \nabla \cdot (M^n \nabla \bar{\mu}^{n+1}) + \alpha \nabla \cdot (M^n \nabla \bar{p}^{n+1}), \tag{49a}$$

$$\begin{aligned} \rho^n \bar{\mu}^{n+1} &= \frac{\rho^{n+1/2}}{\epsilon} g(c^{n+1}, c^n) - \epsilon \nabla \cdot (\rho^{n+1/2} \nabla c^{n+1/2}) \\ &\quad - \alpha \rho^n \rho^{n+1} \left(\frac{G^{n+1/2}}{\epsilon} + \frac{\epsilon}{2} (|\nabla c|^2)^{n+1/2} \right), \end{aligned} \tag{49b}$$

$$\rho^n \frac{\mathbf{u}^{n+1} - \mathbf{u}^n}{\Delta t} + \rho^n (\mathbf{u}^n \cdot \nabla) \mathbf{u}^{n+1} + \frac{1}{2} \left(\frac{\rho^{n+1} - \rho^n}{\Delta t} + \nabla \cdot (\rho^n \mathbf{u}^n) \right) + \frac{1}{\beta} \nabla \bar{p}^{n+1}$$

$$= \frac{1}{\beta} \rho^{n+1} \bar{\mu}^{n+1} \nabla c^{n+1} + \frac{1}{Re} \nabla \cdot (\eta^n (\nabla \mathbf{u}^{n+1} + (\nabla \mathbf{u}^{n+1})^T)) - \frac{2}{3Re} \nabla (\eta^n \nabla \cdot \mathbf{u}^{n+1}), \quad (49c)$$

$$\nabla \cdot \mathbf{u}^{n+1} = \alpha \nabla \cdot (M^n \nabla \bar{\mu}^{n+1}) + \alpha^2 \nabla \cdot (M^n \nabla \bar{p}^{n+1}), \quad (49d)$$

with boundary conditions

$$\frac{c^{n+1} - c^n}{\Delta t} + \mathbf{u}_\tau^{n+1} \cdot \nabla_\Gamma c^{n+1/2} = -M_\Gamma L^{n+1/2}(c), \quad (50a)$$

$$\partial_n \tilde{\mu}^{n+1} = 0, \quad (50b)$$

$$L^{n+1/2}(c) = \epsilon \rho^{n+1/2} \partial_n c^{n+1/2} + \alpha_w \frac{f_w(c^{n+1}) - f_w(c^n)}{c^{n+1} - c^n}, \quad (50c)$$

$$\mathbf{u}^{n+1} \cdot \mathbf{n} = 0, \quad (50d)$$

$$l_s^{-1} \mathbf{u}_{\tau_i}^{s,n+1} = -\mathbf{n} \cdot (\eta^n (\nabla \mathbf{u}^{n+1} + (\nabla \mathbf{u}^{n+1})^T)) \cdot \boldsymbol{\tau}_i + \frac{Re}{\beta} L^{n+1/2} \partial_{\tau_i} c^{n+1/2}, \quad (50e)$$

where $\tilde{\mu}$ is defined in (42b) and we have used the notations

$$(\cdot)^{n+1/2} = \frac{1}{2} [(\cdot)^{n+1} + (\cdot)^n], \quad \rho^{n+1} = \rho(c^{n+1}), \quad (51)$$

$$g(c^{n+1}, c^n) = \frac{1}{4} (c^{n+1} (c^{n+1} - 1) + c^n (c^n - 1)) (c^{n+1} + c^n - 1). \quad (52)$$

We can find that equations (49a), (49d) describe the same system as [42]. The extension we did based on [42] is that we add slip boundary condition (50a), (50c) and (50e) [14,15] to look at the interaction between fluid and the wall. Some numerical results would be shown in section 4.

For above discretization, it satisfies the following properties.

Lemma 3.1. ([51]) *If c^{n+1} is the solution of above system (49)-(50), then we have*

$$G(c^{n+1}) - G(c^n) = g(c^{n+1}, c^n) (c^{n+1} - c^n), \quad (53a)$$

$$\rho(c^{n+1}) - \rho(c^n) = -\alpha \rho^{n+1} \rho^n (c^{n+1} - c^n). \quad (53b)$$

And the system (49)-(50) yields mass conservation for each component of binary fluid

$$\int_{\Omega} \rho^{n+1} d\mathbf{x} = \int_{\Omega} \rho^n d\mathbf{x}, \quad (54a)$$

$$\int_{\Omega} \rho^{n+1} c^{n+1} d\mathbf{x} = \int_{\Omega} \rho^n c^n d\mathbf{x}. \quad (54b)$$

Theorem 3.2. *If $(c^{n+1}, \mu^{n+1}, \mathbf{u}^{n+1}, \bar{p}^{n+1}) \in \mathbf{W}_b$ are solutions of above system (49) with boundary conditions (50), then the following energy law is satisfied:*

$$\begin{aligned} & \mathcal{E}^{n+1, tot} - \mathcal{E}^{n, tot} \\ &= -\frac{\Delta t}{Re} \int_{\Omega} \eta^n \sum_{i < j} |\partial_i u_j^{n+1} + \partial_j u_i^{n+1}|^2 d\mathbf{x} - \frac{2\Delta t}{3Re} \int_{\Omega} \eta^n \sum_{i < j} |\partial_i u_i^{n+1} - \partial_j u_j^{n+1}|^2 d\mathbf{x} \\ & - \frac{\Delta t}{\beta} \int_{\Omega} M^n |\nabla \tilde{\mu}^{n+1}|^2 d\mathbf{x} - \Delta t \int_{\partial\Omega_w} \left(\frac{1}{\beta} M_\Gamma |L^{n+1/2}(c)|^2 + \frac{1}{l_s Re} |\mathbf{u}^{s,n+1}|^2 \right) dS \end{aligned} \quad (55)$$

$$- \Delta t \int_{\partial\Omega_w} \frac{1}{l_s Re} \mathbf{u}^{s,n+1} \cdot \mathbf{u}_w dS, \quad (56)$$

where

$$\mathcal{E}^{n+1, tot} = \int_{\Omega} \frac{\rho^{n+1}}{2} |\mathbf{u}^{n+1}|^2 d\mathbf{x} + \frac{1}{\beta} \int_{\Omega} \rho^{n+1} \left(\frac{1}{\epsilon} G(c^{n+1}) + \frac{\epsilon}{2} |\nabla c^{n+1}|^2 \right) d\mathbf{x} + \frac{\alpha_w}{\beta} \int_{\partial\Omega_w} f_w(c^{n+1}) dS$$

is the discretized total energy.

Proof. Taking inner product of the first equation (49a) with $\frac{\Delta t}{\beta} \bar{\mu}^{n+1}$ results in the following equation

$$\begin{aligned} & \frac{1}{\beta} \int_{\Omega} \rho^n (c^{n+1} - c^n) \bar{\mu}^{n+1} d\mathbf{x} + \frac{\Delta t}{\beta} \int_{\Omega} \rho^{n+1} \mathbf{u}^{n+1} \cdot \nabla c^{n+1} \bar{\mu}^{n+1} d\mathbf{x} \\ &= -\frac{\Delta t}{\beta} \int_{\Omega} M^n \nabla \bar{\mu}^{n+1} \cdot \nabla \bar{\mu}^{n+1} d\mathbf{x}, \end{aligned} \tag{57}$$

where we used the boundary condition (50b) and the definition of $\bar{\mu}$ in (42b).

Multiplying the second equation (49b) with $\frac{c^{n+1}-c^n}{\beta}$ yields [51]

$$\begin{aligned} & \frac{1}{\beta} \int_{\Omega} \rho^n (c^{n+1} - c^n) \bar{\mu}^{n+1} d\mathbf{x} \\ &= \frac{1}{\beta} \int_{\Omega} \rho^{n+1} \left(\frac{1}{\epsilon} G(c^{n+1}) + \frac{\epsilon}{2} |\nabla c^{n+1}|^2 \right) d\mathbf{x} - \frac{1}{\beta} \int_{\Omega} \rho^n \left(\frac{1}{\epsilon} G(c^n) + \frac{\epsilon}{2} |\nabla c^n|^2 \right) d\mathbf{x} \\ & \quad - \frac{1}{\beta} \int_{\partial\Omega_w} \epsilon \rho^{n+1/2} \partial_n c^{n+1/2} (c^{n+1} - c^n) dS, \end{aligned} \tag{58}$$

where we use the results in above lemma and the boundary condition (50a).

Multiplying the Navier-Stokes equation (49c) with $\Delta t \mathbf{u}^{n+1}$, we have

$$\begin{aligned} & \frac{1}{2} \int_{\Omega} (\rho^{n+1} |\mathbf{u}^{n+1}|^2) d\mathbf{x} - \frac{1}{2} \int_{\Omega} (\rho^n |\mathbf{u}^n|^2) d\mathbf{x} \\ &= -\frac{\Delta t}{Re} \int_{\Omega} \eta^n \sum_{i < j} |\partial_i u_j^{n+1} + \partial_j u_i^{n+1}|^2 d\mathbf{x} - \frac{2\Delta t}{3Re} \int_{\Omega} \eta^n \sum_{i < j} |\partial_i u_i^{n+1} - \partial_j u_j^{n+1}|^2 d\mathbf{x} \\ & \quad + \frac{\Delta t}{\beta} \int_{\Omega} \bar{p}^{n+1} \nabla \cdot \mathbf{u}^{n+1} d\mathbf{x} + \frac{\Delta t}{\beta} \int_{\Omega} \rho^{n+1} \bar{\mu}^{n+1} \nabla c^{n+1} \cdot \mathbf{u}^{n+1} d\mathbf{x} \\ & \quad - \frac{\Delta t}{Re} \int_{\partial\Omega_w} l_s^{-1} |\mathbf{u}^{s,n+1}|^2 dS + \frac{\Delta t}{\beta} \int_{\partial\Omega_w} L^{n+1/2} \nabla_{\Gamma} c^{n+1/2} \cdot \mathbf{u}_{\tau}^{n+1} dS, \\ & \quad - \frac{\Delta t}{Re} \int_{\partial\Omega_w} l_s^{-1} \mathbf{u}^{s,n+1} \cdot \mathbf{u}_w dS, \end{aligned} \tag{59}$$

where we used the slip boundary condition (50e) and the tensor calculation in Appendix C.

For the last term in above equation, combining the definition of $L^{n+1/2}$ in (50c) and equation (50a) yields

$$\begin{aligned} & \frac{\Delta t}{\beta} \int_{\partial\Omega_w} L^{n+1/2} \nabla_{\Gamma} c^{n+1/2} \cdot \mathbf{u}_{\tau}^{n+1} dS \\ &= \frac{\Delta t}{\beta} \left(\int_{\partial\Omega_w} \alpha_w \frac{f_w(c^{n+1}) - f_w(c^n)}{c^{n+1} - c^n} \nabla_{\Gamma} c^{n+1/2} \cdot \mathbf{u}_{\tau}^{n+1} dS \right. \\ & \quad \left. + \int_{\partial\Omega} \epsilon \rho^{n+1/2} \partial_n c^{n+1/2} \nabla_{\Gamma} c^{n+1/2} \cdot \mathbf{u}_{\tau}^{n+1} dS \right) \\ &= -\frac{1}{\beta} \int_{\partial\Omega_w} \alpha_w (f_w(c^{n+1}) - f_w(c^n)) dS - \frac{\Delta t}{\beta} \int_{\partial\Omega_w} \alpha_w \frac{f_w(c^{n+1}) - f_w(c^n)}{c^{n+1} - c^n} M_{\Gamma} L^{n+1/2} dS \\ & \quad + \frac{\Delta t}{\beta} \int_{\partial\Omega} \epsilon \rho^{n+1/2} \partial_n c^{n+1/2} \nabla_{\Gamma} c^{n+1/2} \cdot \mathbf{u}_{\tau}^{n+1} dS. \end{aligned} \tag{60}$$

Then equation (59) could be rewritten as

$$\begin{aligned}
 & \frac{1}{2} \int_{\Omega} (\rho^{n+1} |\mathbf{u}^{n+1}|^2) d\mathbf{x} - \frac{1}{2} \int_{\Omega} (\rho^n |\mathbf{u}^n|^2) d\mathbf{x} + \frac{1}{\beta} \int_{\partial\Omega_w} \alpha_w (f_w(c^{n+1}) - f_w(c^n)) dS \\
 &= -\frac{\Delta t}{Re} \int_{\Omega} \eta^n \sum_{i<j} |\partial_i u_j^{n+1} + \partial_j u_i^{n+1}|^2 d\mathbf{x} - \frac{2\Delta t}{3Re} \int_{\Omega} \eta^n \sum_{i<j} |\partial_i u_i^{n+1} - \partial_j u_j^{n+1}|^2 d\mathbf{x} \\
 &+ \frac{\Delta t}{\beta} \int_{\Omega} \bar{p}^{n+1} \nabla \cdot \mathbf{u}^{n+1} d\mathbf{x} + \frac{\Delta t}{\beta} \int_{\Omega} \rho^{n+1} \bar{\mu}^{n+1} \nabla c^{n+1} \cdot \mathbf{u}^{n+1} d\mathbf{x} \\
 &- \frac{\Delta t}{Re} \int_{\partial\Omega_w} l_s^{-1} |\mathbf{u}^{s,n+1}|^2 dS - \frac{\Delta t}{\beta} \int_{\partial\Omega_w} \alpha_w \frac{f_w(c^{n+1}) - f_w(c^n)}{c^{n+1} - c^n} M_{\Gamma} L^{n+1/2} dS \\
 &+ \frac{\Delta t}{\beta} \int_{\partial\Omega} \epsilon \rho^{n+1/2} \partial_n c^{n+1/2} \nabla_{\Gamma} c^{n+1/2} \cdot \mathbf{u}_{\tau}^{n+1} dS - \frac{\Delta t}{Re} \int_{\partial\Omega_w} l_s^{-1} \mathbf{u}^{s,n+1} \cdot \mathbf{u}_w dS.
 \end{aligned} \tag{61}$$

Multiplying the last equation (49d) with $\frac{\Delta t}{\beta} \bar{p}^{n+1}$ yields

$$0 = - \int_{\Omega} \frac{\Delta t}{\beta} \bar{p}^{n+1} \nabla \cdot \mathbf{u}^{n+1} d\mathbf{x} - \frac{\Delta t}{\beta} \int_{\Omega} M^n \nabla \bar{\mu}^{n+1} \cdot \nabla \bar{p}^{n+1} d\mathbf{x}. \tag{62}$$

Summing up equations (57), (58), (61) and (62) results

$$\begin{aligned}
 & \mathcal{E}^{n+1,tot} - \mathcal{E}^{n,tot} \\
 &= -\frac{\Delta t}{Re} \int_{\Omega} \eta^n \sum_{i<j} |\partial_i u_j^{n+1} + \partial_j u_i^{n+1}|^2 d\mathbf{x} - \frac{2\Delta t}{3Re} \int_{\Omega} \eta^n \sum_{i<j} |\partial_i u_i^{n+1} - \partial_j u_j^{n+1}|^2 d\mathbf{x} \\
 &- \frac{\Delta t}{\beta} \int_{\Omega} M^n |\nabla \bar{\mu}^{n+1}|^2 d\mathbf{x} - \int_{\partial\Omega_w} \frac{\Delta t}{l_s Re} |\mathbf{u}^{s,n+1}|^2 dS - \int_{\partial\Omega_w} \frac{\Delta t}{l_s Re} \mathbf{u}^{s,n+1} \cdot \mathbf{u}_w dS \\
 &- \frac{\Delta t}{\beta} \int_{\partial\Omega_w} \alpha_w \frac{f_w(c^{n+1}) - f_w(c^n)}{c^{n+1} - c^n} M_{\Gamma} L^{n+1/2} dS \\
 &+ \frac{1}{\beta} \int_{\partial\Omega_w} \epsilon \rho^{n+1/2} \partial_n c^{n+1/2} (c^{n+1} - c^n) dS + \frac{\Delta t}{\beta} \int_{\partial\Omega} \epsilon \rho^{n+1/2} \partial_n c^{n+1/2} \nabla_{\Gamma} c^{n+1/2} \cdot \mathbf{u}_{\tau}^{n+1} dS \\
 &= -\frac{\Delta t}{Re} \int_{\Omega} \eta^n \sum_{i<j} |\partial_i u_j^{n+1} + \partial_j u_i^{n+1}|^2 d\mathbf{x} - \frac{2\Delta t}{3Re} \int_{\Omega} \eta^n \sum_{i<j} |\partial_i u_i^{n+1} - \partial_j u_j^{n+1}|^2 d\mathbf{x} \\
 &- \frac{\Delta t}{\beta} \int_{\Omega} M^n |\nabla \bar{\mu}^{n+1}|^2 d\mathbf{x} - \int_{\partial\Omega_w} \frac{\Delta t}{l_s Re} |\mathbf{u}^{s,n+1}|^2 dS - \int_{\partial\Omega_w} \frac{\Delta t}{l_s Re} \mathbf{u}^{s,n+1} \cdot \mathbf{u}_w dS \\
 &- \frac{\Delta t}{\beta} \int_{\partial\Omega_w} \alpha_w \frac{f_w(c^{n+1}) - f_w(c^n)}{c^{n+1} - c^n} M_{\Gamma} L^{n+1/2} dS - \frac{\Delta t}{\beta} \int_{\partial\Omega_w} \epsilon \rho^{n+1/2} \partial_n c^{n+1/2} M_{\Gamma} L^{n+1/2} dS \\
 &= -\frac{\Delta t}{Re} \int_{\Omega} \eta^n \sum_{i<j} |\partial_i u_j^{n+1} + \partial_j u_i^{n+1}|^2 d\mathbf{x} - \frac{2\Delta t}{3Re} \int_{\Omega} \eta^n \sum_{i<j} |\partial_i u_i^{n+1} - \partial_j u_j^{n+1}|^2 d\mathbf{x} \\
 &- \frac{\Delta t}{\beta} \int_{\Omega} M^n |\nabla \bar{\mu}^{n+1}|^2 d\mathbf{x} - \int_{\partial\Omega_w} \frac{\Delta t}{l_s Re} |\mathbf{u}^{s,n+1}|^2 dS - \frac{\Delta t}{\beta} \int_{\partial\Omega_w} M_{\Gamma} |L^{n+1/2}|^2 dS \\
 &- \int_{\partial\Omega_w} \frac{\Delta t}{l_s Re} \mathbf{u}^{s,n+1} \cdot \mathbf{u}_w dS,
 \end{aligned} \tag{63}$$

where we used the definition of $\bar{\mu}$ (42b) and slip boundary condition (50e). □

Newton’s method [51,65] is utilized to solve the above nonlinear system (49)-(50).

Remark 3.1. This discrete scheme is first order accuracy. Higher order schemes can be derived as in [65,63] or by approximating energies through IEQ/SAV formulations [74,75,58].

Remark 3.2. The scheme is highly nonlinear and fully implicitly coupled since we would like to ensure that the discrete energy law as same as the continuous version, i.e. the equality. A proof of the unique solvability of the discrete scheme could be as hard as that for the original PDEs. Most of existing studies on the solvability of Cahn-Hilliard system [76–78], are done by using the linearization (convex splitting) treatments which highly reduce the nonlinearity. In this paper, Newton’s method [65,51] is utilized to solve the nonlinear discrete system, and the solvability of a Newton iteration or Newton linearization is possible if Δt is sufficiently small.

3.2. Fully-discrete C^0 finite element scheme

The fully-discrete C^0 finite element scheme for this time-discrete primitive scheme (49)-(50) is presented in the section. For simplicity, we only consider a two-dimensional case here. It is straightforward to extend the results to three-dimensional case. The domain Ω is a bounded domain with Lipschitz-continuous boundary $\partial\Omega$. Specifically, we denote $\partial\Omega_w$ as the solid wall where the slip boundary condition is used. Let $\mathbf{W}_b^h = H^h \times H^h \times \mathbf{U}_b^h \times P^h$ be the finite dimensional space of \mathbf{W}_b based on a given finite element discretization of Ω . If we assume that $\rho^n \in L^\infty(\Omega)$ and positive [65], then the weak form of semi-discrete system (49) with boundary conditions (50) is the following: finding $(c_h^{n+1}, \bar{\mu}_h^{n+1}, \mathbf{u}_h^{n+1}, \bar{p}_h^{n+1}) \in \mathbf{W}_b^h$, such that

$$\begin{aligned} & \int_{\Omega} \left(\rho_h^n \frac{c_h^{n+1} - c_h^n}{\Delta t} + \rho_h^{n+1} (\mathbf{u}_h^{n+1} \cdot \nabla) c_h^{n+1} \right) \psi_h d\mathbf{x} \\ &= - \int_{\Omega} M^n \left(\nabla \bar{\mu}_h^{n+1} + \alpha \nabla \bar{p}_h^{n+1} \right) \cdot \nabla \psi_h d\mathbf{x}, \end{aligned} \tag{64a}$$

$$\begin{aligned} & \int_{\Omega} \rho_h^n \bar{\mu}_h^{n+1} \chi_h d\mathbf{x} = \int_{\Omega} \frac{\rho_h^{n+1/2}}{\epsilon} g(c_h^{n+1}, c_h^n) \chi_h d\mathbf{x} + \int_{\Omega} \epsilon \rho_h^{n+1/2} \nabla c_h^{n+1/2} \cdot \nabla \chi_h d\mathbf{x} \\ & - \int_{\Omega} \alpha \rho_h^n \rho_h^{n+1} \left(\frac{G_h^{n+1/2}}{\epsilon} + \frac{\epsilon}{2} (|\nabla c_h|^2)^{n+1/2} \right) \chi_h d\mathbf{x} - \int_{\partial\Omega_w} \epsilon \rho_h^{n+1/2} \partial_n c_h^{n+1/2} \chi_h dS, \end{aligned} \tag{64b}$$

$$\begin{aligned} & \int_{\Omega} \left\{ \rho_h^n \frac{\mathbf{u}_h^{n+1} - \mathbf{u}_h^n}{\Delta t} + \rho_h^n (\mathbf{u}_h^n \cdot \nabla) \mathbf{u}_h^{n+1} + \frac{1}{2} \left(\frac{\rho_h^{n+1} - \rho_h^n}{\Delta t} + \nabla \cdot (\rho_h^n \mathbf{u}_h^n) \right) \right\} \cdot \mathbf{v}_h d\mathbf{x} \\ &= - \frac{1}{\beta} \int_{\Omega} \nabla \bar{p}_h^{n+1} \cdot \mathbf{v}_h d\mathbf{x} + \int_{\Omega} \frac{1}{\beta} \rho_h^{n+1} \bar{\mu}_h^{n+1} \nabla c^{n+1} \cdot \mathbf{v}_h d\mathbf{x} \\ & - \frac{1}{Re} \int_{\Omega} (\eta^n (\nabla \mathbf{u}_h^{n+1} - (\nabla \mathbf{u}_h^{n+1})^T)) : \nabla \mathbf{v}_h d\mathbf{x} + \frac{2}{3Re} \int_{\Omega} \eta^n \nabla \cdot \mathbf{u}_h^{n+1} \nabla \cdot \mathbf{v}_h d\mathbf{x} \\ & - \int_{\partial\Omega_w} \frac{1}{Re l_s} \mathbf{u}_h^{s,n+1} \cdot \mathbf{v}_h dS + \int_{\partial\Omega} \frac{1}{\beta} L_h^{n+1/2} \nabla_{\Gamma} c_h^{n+1/2} \cdot \mathbf{v}_h dS, \end{aligned} \tag{64c}$$

$$- \int_{\Omega} \nabla q_h \cdot \mathbf{u}_h^{n+1} = -\alpha \int_{\Omega} M^n \left(\nabla \bar{\mu}_h^{n+1} + \alpha \nabla \bar{p}_h^{n+1} \right) \cdot \nabla q_h d\mathbf{x}, \tag{64d}$$

for any $(\psi_h, \chi_h, \mathbf{v}_h, q_h) \in \mathbf{W}_0^h$.

Lemma 3.3. The fully discretized system (64) satisfies mass conservation for each component of binary fluid

$$\int_{\Omega} \rho_h^{n+1} d\mathbf{x} = \int_{\Omega} \rho_h^n d\mathbf{x}, \tag{65a}$$

$$\int_{\Omega} \rho_h^{n+1} c_h^{n+1} d\mathbf{x} = \int_{\Omega} \rho_h^n c_h^n d\mathbf{x}. \tag{65b}$$

Proof. Setting $\psi_h = q_h = \rho_h^{n+1}$ in Eqs. (64a) and (64d), we have

$$\begin{aligned} & \int_{\Omega} \left(\rho_h^n \rho_h^{n+1} \frac{c_h^{n+1} - c_h^n}{\Delta t} + (\rho_h^{n+1})^2 (\mathbf{u}_h^{n+1} \cdot \nabla) c_h^{n+1} \right) d\mathbf{x} \\ &= - \int_{\Omega} M^n \left(\nabla \bar{\mu}_h^{n+1} + \alpha \nabla \bar{p}_h^{n+1} \right) \cdot \nabla \rho_h^{n+1} d\mathbf{x}, \\ & - \frac{1}{\alpha} \int_{\Omega} \nabla \rho_h^{n+1} \cdot \mathbf{u}_h^{n+1} d\mathbf{x} = \int_{\Omega} M^n \left(\nabla \bar{\mu}_h^{n+1} + \alpha \nabla \bar{p}_h^{n+1} \right) \cdot \nabla \rho_h^{n+1} d\mathbf{x}. \end{aligned}$$

Adding the above two equations and using Eqs. (10) and (53b) yields

$$\int_{\Omega} \left(\frac{\rho_h^{n+1} - \rho_h^n}{\Delta t} + \nabla \cdot (\rho_h^{n+1} \mathbf{u}_h^{n+1}) \right) d\mathbf{x} = 0. \tag{66}$$

Using the boundary condition $\mathbf{u}_h^{n+1} \cdot \mathbf{n} = 0$, we have the conservation of total mass

$$\int_{\Omega} (\rho_h^{n+1} - \rho_h^n) d\mathbf{x} = 0. \tag{67}$$

Choosing $\psi_h = q_h = \hat{\rho}_h^{n+1} c_h^{n+1}$ in Eqs. (64a) and (64d), similarly we have

$$\int_{\Omega} \left(\frac{\rho_h^{n+1} - \rho_h^n}{\Delta t} c_h^{n+1} + \nabla \cdot (\rho_h^{n+1} \mathbf{u}_h^{n+1}) \right) c_h^{n+1} d\mathbf{x} = 0. \tag{68}$$

Choosing $\psi_h = 1$ in Eq. (64a) yields

$$\int_{\Omega} \left(\rho_h^n \frac{c_h^{n+1} - c_h^n}{\Delta t} + \rho_h^{n+1} (\mathbf{u}_h^{n+1} \cdot \nabla) c_h^{n+1} \right) d\mathbf{x} = 0. \tag{69}$$

Adding the above two equations and using the velocity boundary condition $\mathbf{u}_h^{n+1} \cdot \mathbf{n} = 0$, we have

$$\int_{\Omega} (\rho_h^{n+1} c_h^{n+1} - \rho_h^n c_h^n) d\mathbf{x} = 0. \quad \square$$

Theorem 3.4. If $(c_h^{n+1}, \bar{\mu}_h^{n+1}, \mathbf{u}_h^{n+1}, \bar{p}_h^{n+1})$ are solutions of the above system (64), then the following energy law is satisfied:

$$\begin{aligned} & \mathcal{E}_h^{n+1, \text{tot}} - \mathcal{E}_h^{n, \text{tot}} \\ &= - \frac{\Delta t}{Re} \int_{\Omega} \eta_h^n \sum_{i < j} |\partial_i u_{h,j}^{n+1} + \partial_j u_{h,i}^{n+1}|^2 d\mathbf{x} - \frac{2\Delta t}{3Re} \int_{\Omega} \eta_h^n \sum_{i < j} |\partial_i u_{h,i}^{n+1} - \partial_j u_{h,j}^{n+1}|^2 d\mathbf{x} \\ & - \frac{\Delta t}{\beta} \int_{\Omega} M^n |\nabla \bar{\mu}_h^{n+1}|^2 d\mathbf{x} - \Delta t \int_{\partial\Omega_w} \left(\frac{1}{\beta} M_{\Gamma} |L_h^{n+1/2}(c_h)|^2 + \frac{1}{l_s Re} |\mathbf{u}_h^{s, n+1}|^2 \right) dS \\ & - \Delta t \int_{\partial\Omega_w} \frac{1}{l_s Re} \mathbf{u}_h^{s, n+1} \cdot \mathbf{u}_w dS \end{aligned} \tag{70}$$

where

$$\mathcal{E}_h^{n+1} = \int_{\Omega} \frac{\rho_h^{n+1} |\mathbf{u}_h^{n+1}|^2}{2} d\mathbf{x} + \frac{1}{\beta} \int_{\Omega} \rho_h^{n+1} \left(\frac{1}{\epsilon} G(c_h^{n+1}) + \frac{\epsilon}{2} |\nabla c_h^{n+1}|^2 \right) d\mathbf{x} + \frac{\alpha_w}{\beta} \int_{\partial\Omega_w} f_w(c_h^{n+1}) dS$$

is the discretized total energy.

It can be proved by choosing

$$\psi_h = \frac{\Delta t}{\beta} \bar{\mu}_h^{n+1}, \quad \chi_h = \frac{c_h^{n+1} - c_h^n}{\beta}, \quad \mathbf{v}_h = \Delta t \mathbf{u}_h^{n+1}, \quad q_h = \frac{\Delta t}{\beta} \bar{p}_h^{n+1} \tag{71}$$

in Eq. (64) and following the proof of Theorem 3.2.

4. Simulation results

In this section, we present some numerical simulations using the aforementioned algorithm. Three cases are considered: Couette flow, moving droplets in shear flow and rising bubbles to illustrate the convergence rate, the effect of contact angle and the quasi-incompressibility of two-phase flow with large density ratio, respectively. All of the numerical simulations in this part are based on the proposed finite element scheme and implemented with the FreeFem++ [79].

4.1. Convergence study: Couette flow

We start with convergence test using Couette flow with different density and viscosity [56,58] as in Fig. 2. The domain size is $[0, 0.6] \times [0, 0.1]$. The top and bottom walls move oppositely with $\mathbf{u}_w = (1, 0)^T$. We do the convergence study for two-phase fluids with both low and high density ratios.

For the case of low density ratio, the parameters are listed as follows:

$$\begin{aligned} Re = 200, \beta = 10, M = 2.5 \times 10^{-8}, \epsilon = 0.01, \alpha_w = 4.17 \times 10^{-3}, \rho_1 = 0.8, \rho_2 = 1, \\ \eta_1 = \eta_2 = 1, \theta_s = 120^\circ, M_\Gamma = 5 \times 10^5, \\ l_{s1} = l_{s2} = 0.01, \Delta t = 1 \times 10^{-3}. \end{aligned}$$

We first present the convergence study for P^1 element with $h = 1/80, 1/120, 1/180, 1/270$ and P^2 element with $h = 1/40, 1/60, 1/90, 1/135$ (Table 1). The results with $h = 1/400$ and $1/200$ are used as the reference solutions for P^1 and P^2 elements, respectively.

For the case of high density ratio, the parameters are listed as follows:

$$\begin{aligned} Re = 20, \beta = 1.67 \times 10^{-2}, M = 3 \times 10^{-9}, \rho_1 = 0.01, \rho_2 = 1, \\ \eta_1 = 0.01, \eta_2 = 1, \epsilon = 1.5 \times 10^{-3}, \alpha_w = 8.33 \times 10^{-8}, \theta_s = 120^\circ, M_\Gamma = 5 \times 10^5, \end{aligned}$$

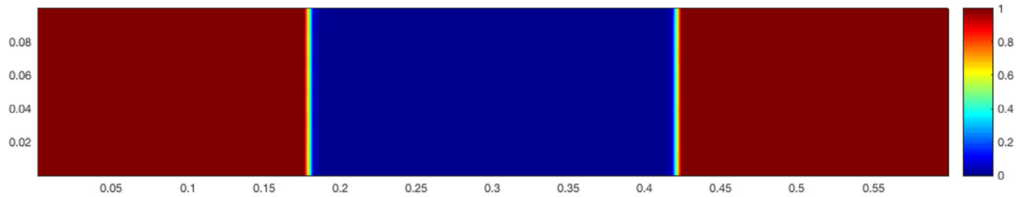


Fig. 2. Initial condition of phase 1 concentration c for the two phase Couette flow. Phase 1 fluid is put on two-sides and phase 2 is put in the middle. Positions a and b are two contact points on the bottom walls. (For interpretation of the colors in the figure(s), the reader is referred to the web version of this article.)

Table 1

L^2 norm of the error and convergence rate for velocity $\mathbf{u} = (u_x, u_y)$, phase function c , at time $t = 0.2$ with density ratio $\rho_1 : \rho_2 = 0.8 : 1$ viscosity ratio $\eta_1 : \eta_2 = 1 : 1$.

Space step h	P^1 element					
	Err(u_x)	Rate	Err(u_y)	Rate	Err(c)	Rate
1/80	1.7e-3		2.3e-4		2.3e-4	
1/120	8.0e-4	1.88	1.0e-4	2.08	1.2e-4	1.69
1/180	3.6e-4	1.95	4.1e-5	2.20	5.8e-5	1.76
1/270	1.6e-4	1.99	1.5e-5	2.49	3.0e-5	1.64
Space step h	P^2 element					
	Err(u_x)	Rate	Err(u_y)	Rate	Err(c)	Rate
1/40	1.1e-3		2.2e-4		2.7e-4	
1/60	4.5e-4	2.26	7.0e-5	2.82	1.0e-4	2.36
1/90	1.7e-4	2.49	2.1e-5	2.92	3.8e-5	2.43
1/135	5.1e-5	2.92	6.6e-6	2.89	1.3e-5	2.65

Table 2
 L^2 norm of the error and convergence rate for velocity $\mathbf{u} = (u_x, u_y)$, phase function c , at time $T = 0.1$ with density ratio $\rho_1 : \rho_2 = 0.01 : 1$, viscosity ratio $\eta_1 : \eta_2 = 0.01 : 1$.

Space step h	P^1 element					
	Err(u_x)	Rate	Err(u_y)	Rate	Err(c)	Rate
1/80	1.9e-3		1.7e-4		6.4e-4	
1/120	9.8e-4	1.68	7.2e-5	2.08	3.5e-4	1.51
1/180	4.7e-4	1.82	2.9e-5	2.48	1.7e-4	1.79
1/270	1.9e-4	2.27	1.0e-5	2.56	7.2e-5	2.14
Space step h	P^2 element					
	Err(u_x)	Rate	Err(u_y)	Rate	Err(c)	Rate
1/40	1.4e-3		1.3e-4		3.9e-4	
1/60	6.5e-4	1.98	4.1e-5	2.91	1.9e-4	1.80
1/90	2.7e-4	2.20	1.2e-5	2.95	7.7e-5	2.23
1/135	5.1e-5	2.77	3.9e-6	2.83	2.8e-5	2.46

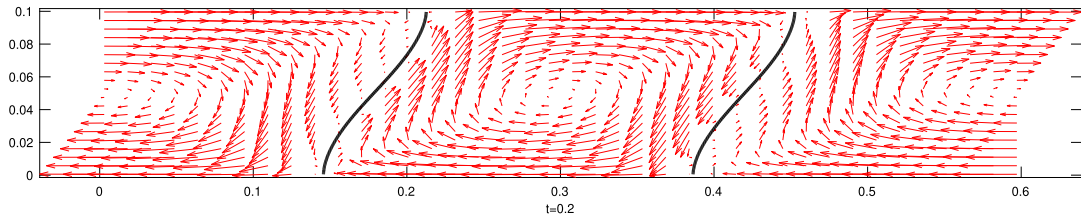


Fig. 3. The interface and velocity profile at $T = 0.2$, high density ratio $\rho_1 = 0.01$, $\rho_2 = 1$.

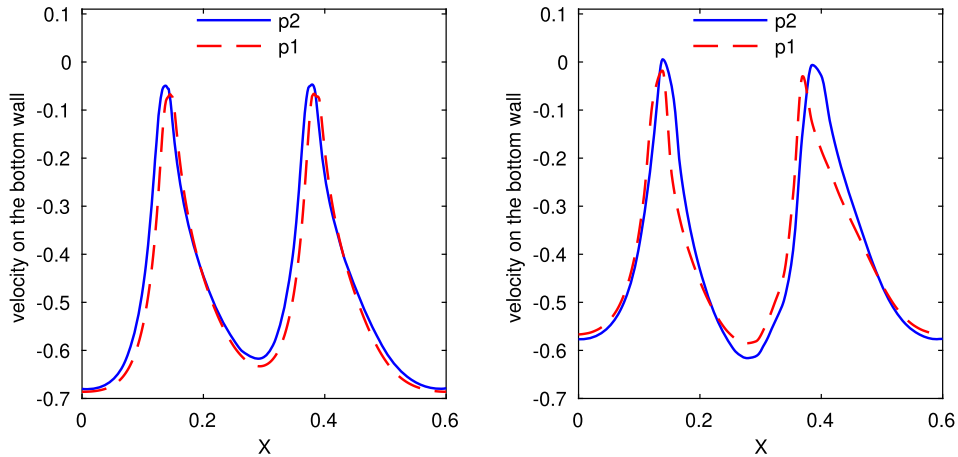


Fig. 4. Velocity on wall around equilibrium state. Left: low density ratio $\rho_1 = 0.8$, $\rho_2 = 1$; Right: large density ratio $\rho_1 = 0.01$, $\rho_2 = 1$.

$$l_{s1} = 1.33, l_{s2} = 0.1, \Delta t = 0.25 \times 10^{-3}.$$

The convergence rate for both P^1 element and P^2 element are shown in Table 2. It illustrates the 2nd-order for P^1 element and 3rd-order for P^2 element convergence rate in the sense of L^2 norm.

The profile of interface and velocity fields around steady state are shown in Fig. 3.

The fluid velocities on the wall are shown in Fig. 4. It shows that for both low and high density ratio case, P^1 element could yield consistent contact velocity with P^2 element.

In Fig. 5, we check the L^2 norm of $\nabla \cdot \mathbf{u}$ with different ϵ . The results confirm that as ϵ decreases, the solution converges to the sharp interface incompressible fluids.

In Fig. 6, we check the total mass convergence of each phase in Lemma 3.3 for both low and high density ratios. It confirms that P^1 and P^2 elements could preserve the mass very well in both cases.

Then we set the wall velocity $\mathbf{u}_w = (0, 0)^T$ to check the evolution of the total free energy when there is no input energy from outside. It is shown in Fig. 7 that the free energy decreases over time for both methods and two density ratios, indicating that our schemes are energy stable.

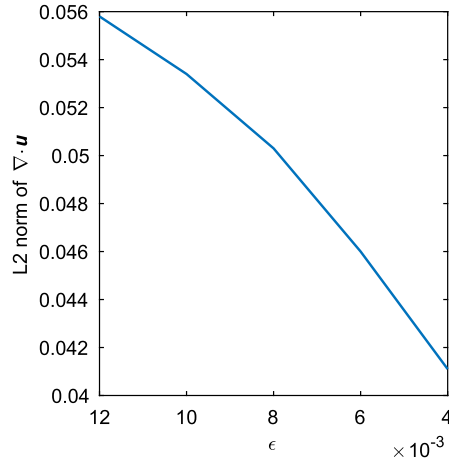


Fig. 5. L^2 norm of $\nabla \cdot \mathbf{u}$ with different ϵ .

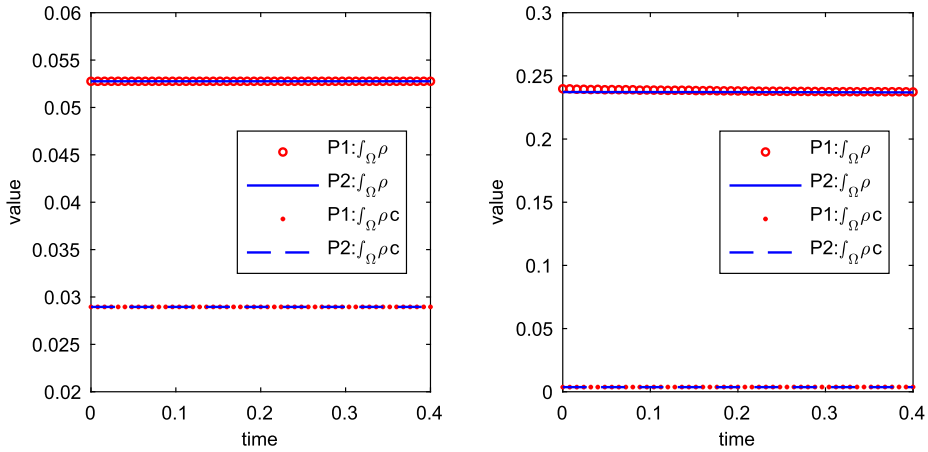


Fig. 6. Mass conservation for each component. Left: low density ratio; Right: high density ratio.

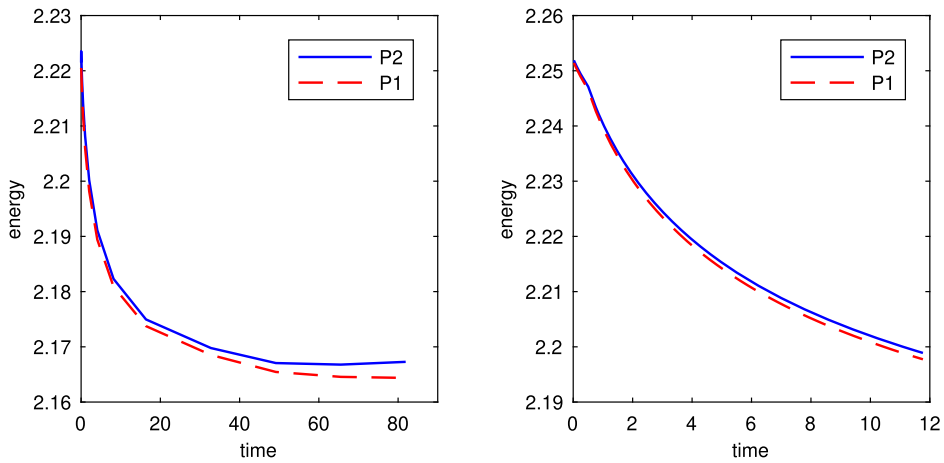


Fig. 7. Total energy as a function of time. Left: lower density ratio; Right: high density ratio.

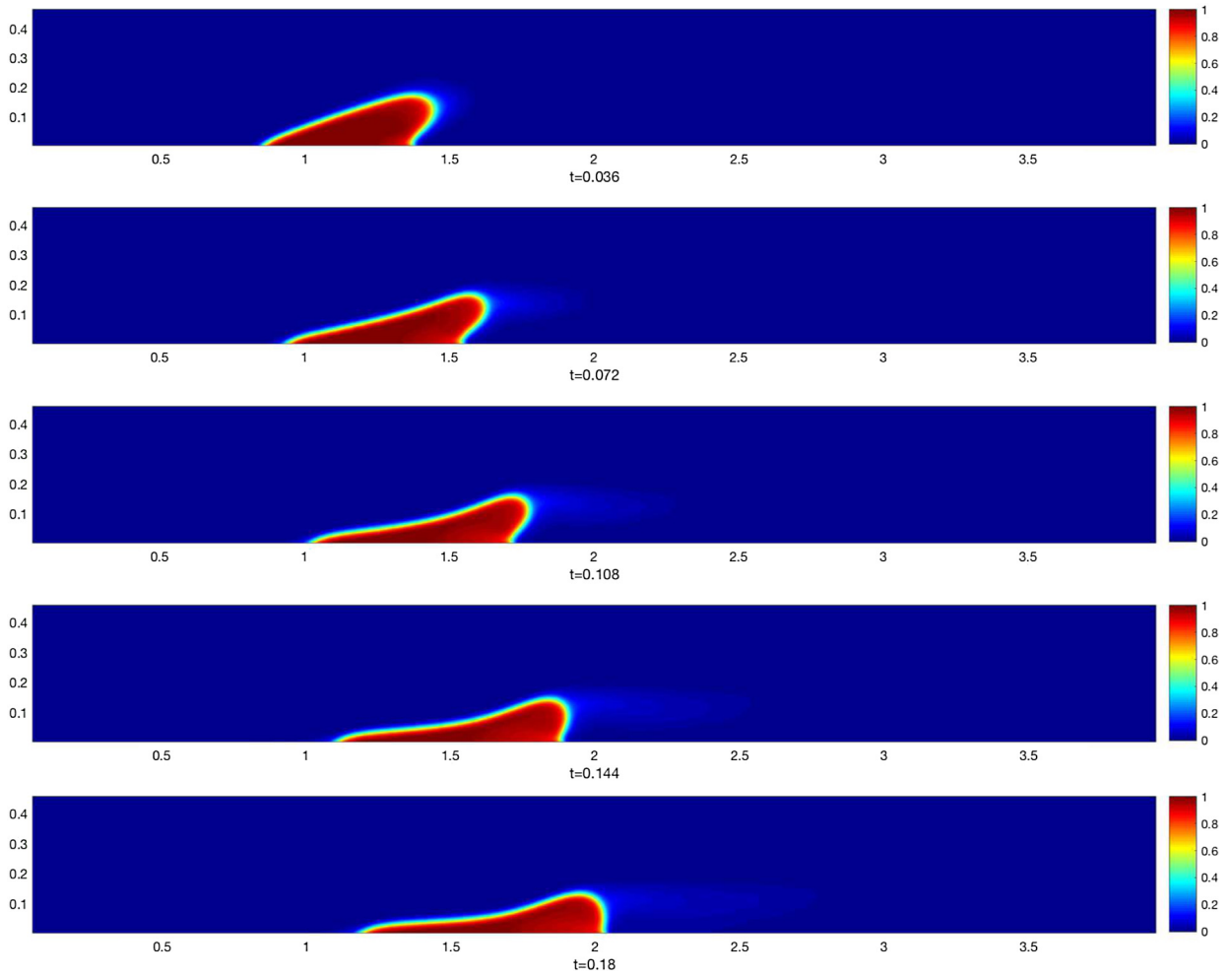


Fig. 8. Moving droplet in shear flow with acute static contact angle $\theta_s = 60^\circ$.

4.2. Contact angle effect: moving droplet

In this example, we show the dynamics of an oil droplet in water with shear flow. The density ratio is $\rho_1 : \rho_2 = 0.8 : 1$ and viscosity ratio is $\eta_1 : \eta_2 = 1 : 1$. The other parameters are as follows

$$Re = 5, \beta = 7.14 \times 10^{-3}, M = 2.8 \times 10^{-4}, \epsilon = 0.005, \alpha_w = 0.129,$$

$$M_\Gamma = 5 \times 10^8, l_s = 6.667 \times 10^{-5}.$$

The domain size is $[0, 4] \times [0, 0.5]$ with adaptive mesh and $\Delta t = 4 \times 10^{-4}$. The initial profile is set to be a half circle

$$c_0 = 0.5 - 0.5 \tanh\left(\frac{\sqrt{(x-1)^2 + y^2} - 0.2}{\sqrt{2}\epsilon}\right).$$

In Figs. 8 and 10, the profiles of droplets under shear flow at different time are presented. For the acute contact angle case (Fig. 8), the droplet is elongated by the shear flow force and hydrophilic force on the wall. The distance between two contact points increases over time (see Fig. 11, black curve) as a spreading droplet. While for the obtuse case (see Fig. 10), the hydrophobic force induced the shrink of contact lines on the wall. The distance between two contact points keeps decreasing (see Fig. 11, blue curve). With the help of shear force, the droplet eventually detaches from the wall around $t = 0.1$ and get stabilized at the center of the flow. When the contact angle is 90° (Fig. 9), the competition between wall attraction force and bulk shear force first elongates the droplet and finally breaks the bubble around time $t = 0.15$.

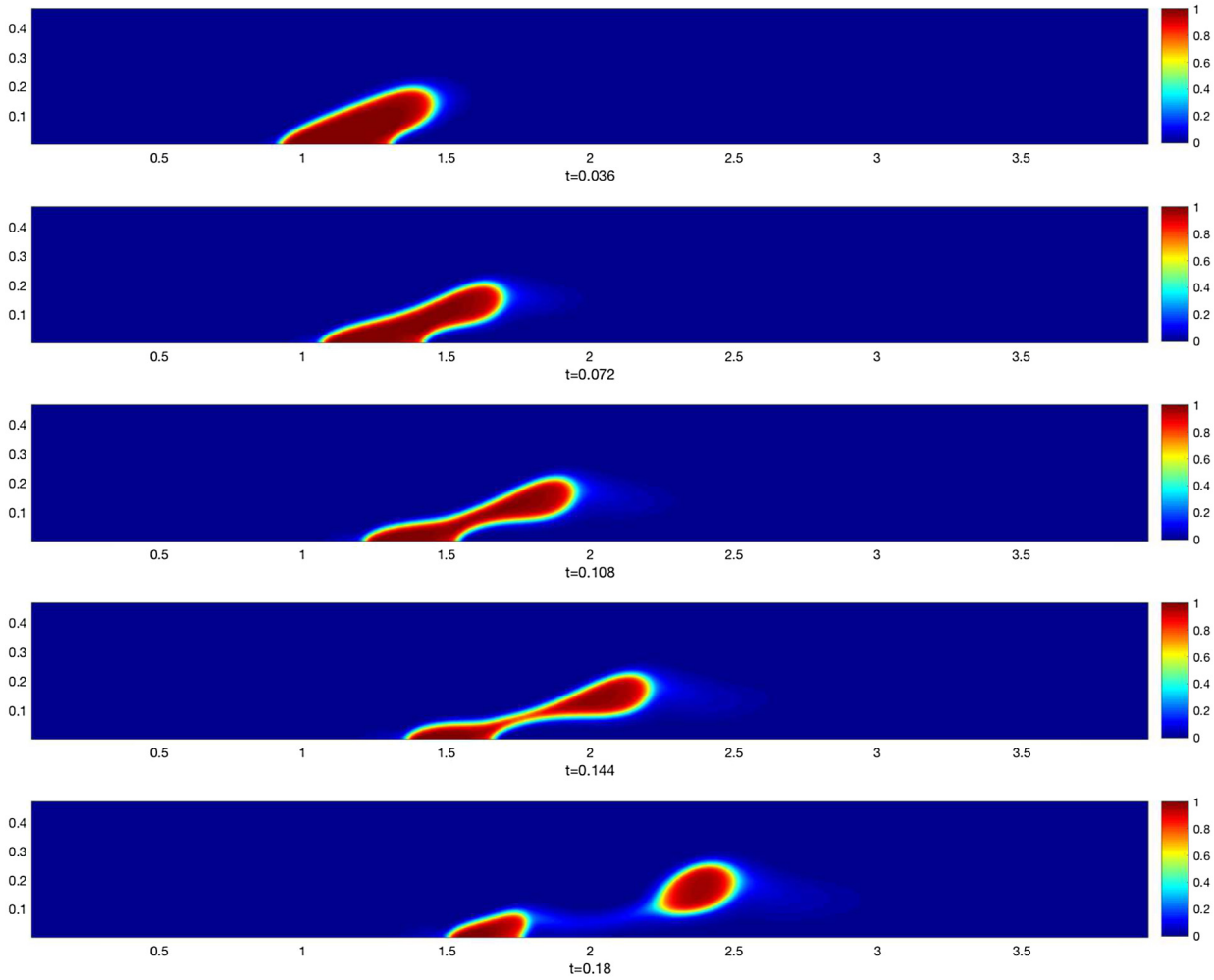


Fig. 9. Moving droplet in shear flow with acute static contact angle $\theta_s = 90^\circ$.

4.3. Large density ratio: rising bubble

As a last example, we carry out numerical simulation of an air bubble raising in water. The density ratio is set to be $\rho_1 : \rho_2 = 0.001 : 1$ and viscosity ratio is $\eta_1 : \eta_2 = 0.01 : 1$. The domain size is $(x, y) \in [0, 0.15] \times [0, 0.15]$ with mesh size $h = 1/540$ and timestep $\Delta t = 2 \times 10^{-4}$. Parameters are listed as follows

$$Re = 300, \beta = 0.09, M = 6.67 \times 10^{-17}, \epsilon = 0.01, \alpha_w = 100, \\ M_\Gamma = 5 \times 10^8, l_s = 0.04.$$

The initial profile is set to be a half circle with radius 0.05 and center at $(0.075, 0)$:

$$c_0 = 0.5 - 0.5 \tanh \left(\frac{\sqrt{(x - 0.075)^2 + y^2} - 0.05}{\sqrt{2}\epsilon} \right)$$

The snapshots of interfaces with velocity fields and $\nabla \cdot \mathbf{u}$ profiles for bubbles with acute contact angle $\theta_s = 60^\circ$ and obtuse contact angle $\theta_s = 120^\circ$ are presented in Figs. 12 and 13, respectively. When the angle is acute, the attractive (hydrophilic) force from the wall competes with the buoyancy force and break the bubble. While for the obtuse case, the wall repulsive (hydrophobic) fore enhances the bubble rising under buoyancy force. The $\nabla \cdot \mathbf{u}$ profiles confirm that the quasi-incompressible property of two-phase fluid with different density only happens around the interface due to the slightly mixing [51].

In Fig. 14, we show the dynamics of rising velocity $V_c = \frac{\int_{\Omega} u_y c dx}{\int_{\Omega} c dx}$ of bubble with different static contact angles. The vertical dash lines are the time when bubbles break ($\theta_s = 60^\circ, 90^\circ$) or fully detach ($\theta_s = 120^\circ$) from wall. It shows that the hydrophobic bubble (blue line, $\theta_s = 120^\circ$) has a larger acceleration to form a sealing bubble. At $t = 0.0384$, the bubble fully

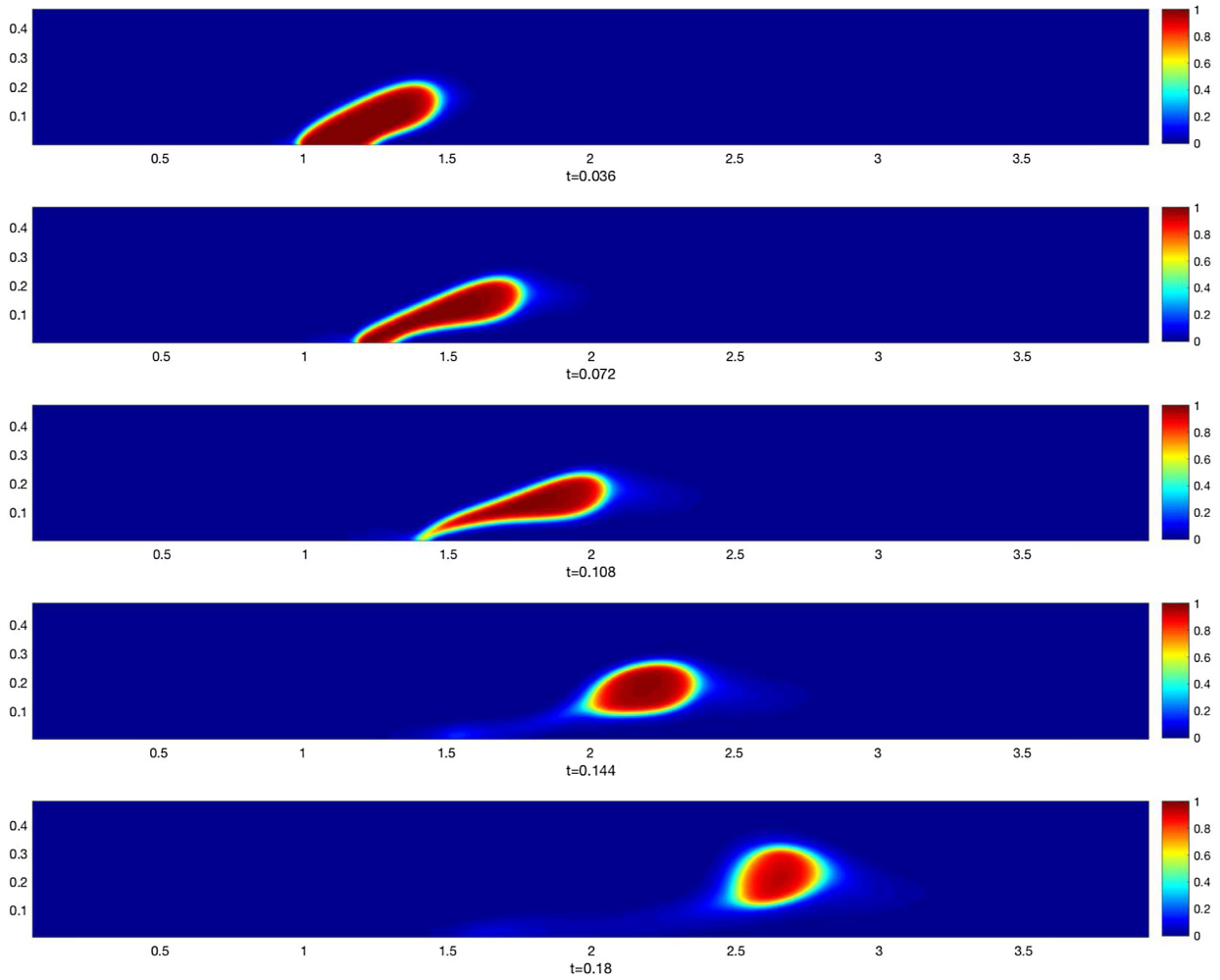


Fig. 10. Moving droplet in shear flow with obtuse static contact angle $\theta_s = 120^\circ$.

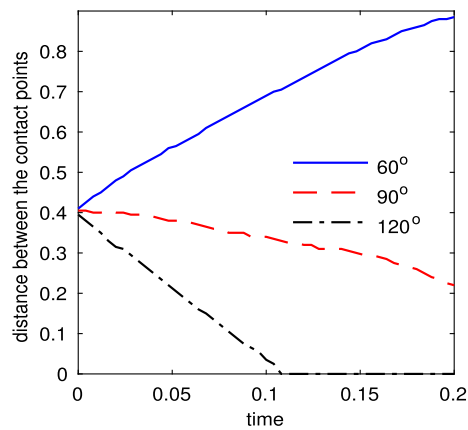


Fig. 11. Moving droplet in shear flow: dynamics of the distance between two contact points.

detaches from the wall. For the hydrophilic bubbles, in the beginning, the velocity increases slowly due to the competition between the hydrophilic force, the surface tension and the buoyancy force. The bubble is stretched into a tear shape which induces a larger velocity around the narrow neck region (see Fig. 12). The maximum velocity is achieved around the break time because the instantaneous response of the surface tension to the large surface deformation.

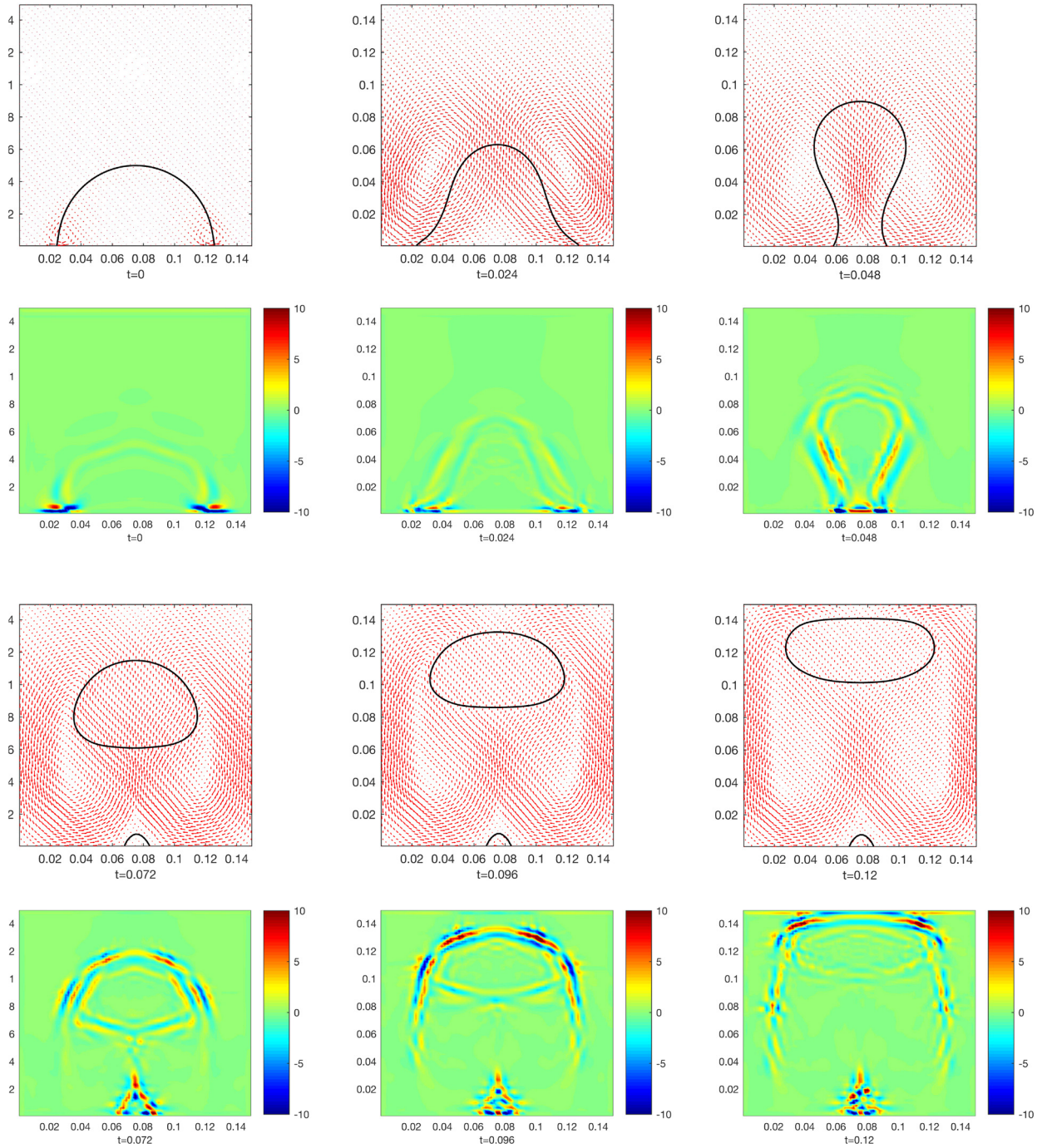


Fig. 12. Rising bubble interface with velocity field (first and third rows) and $\nabla \cdot \mathbf{u}$ (second and fourth rows) at different time when $\theta_s = 60^\circ$.

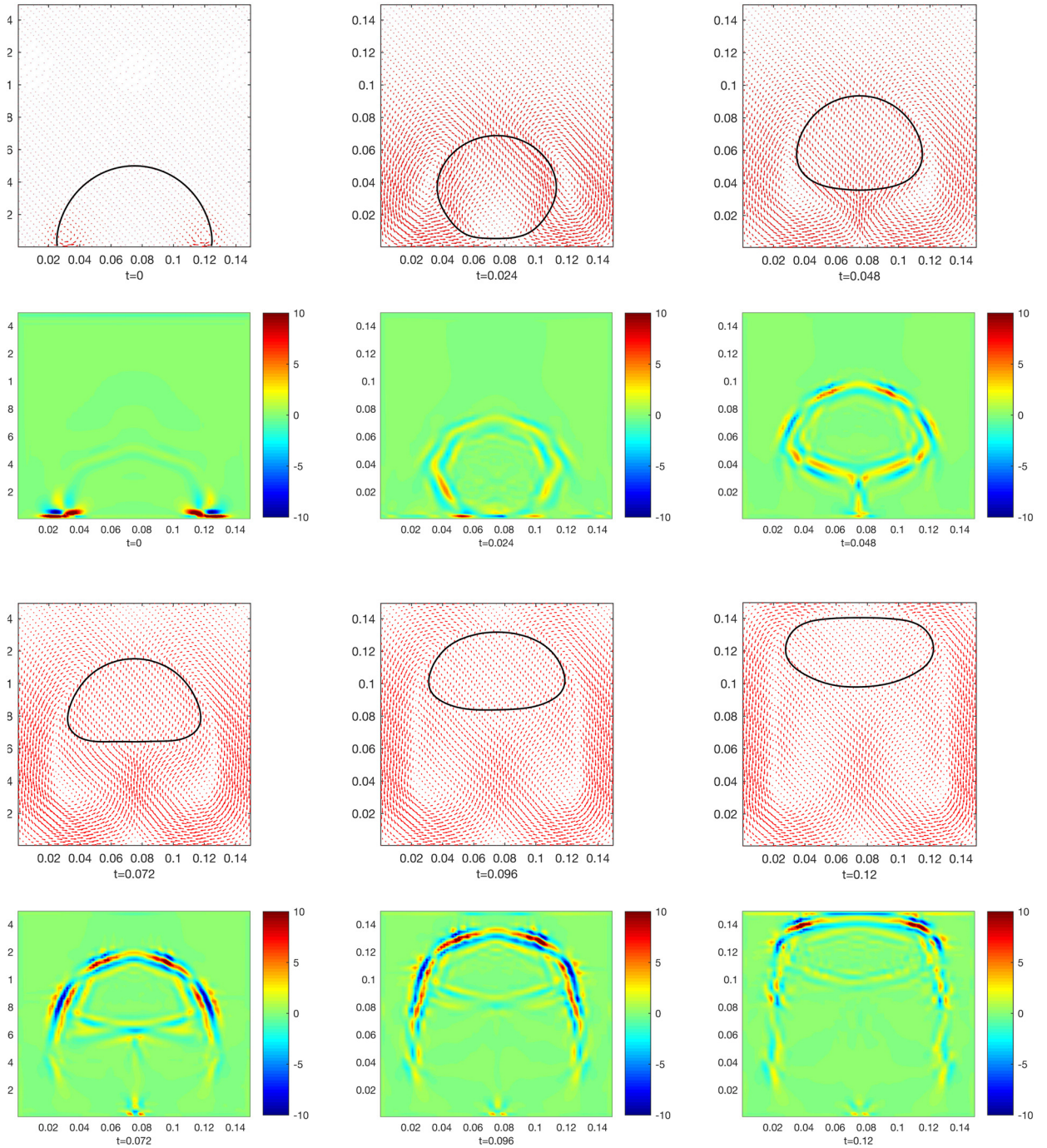


Fig. 13. Rising bubble interface with velocity field (first and third rows) and $\nabla \cdot \mathbf{u}$ (second and fourth rows) at different time when $\theta_b = 120^\circ$.

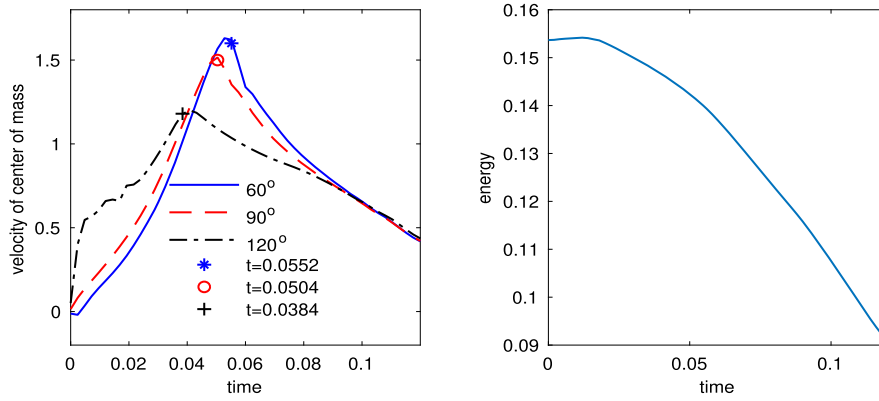


Fig. 14. Rising velocity and energy decay. Left: Solid lines are rising velocity and vertical dash lines are time when bubble break or full removed from wall. Black: $\theta = 60^\circ$ with break time $t = 0.0552$; Red: $\theta = 90^\circ$ with break time $t = 0.0504$; Blue: $\theta = 120^\circ$ with removed time $t = 0.0384$. Right: the energy decay when $\theta = 120^\circ$.

5. Conclusion

In this paper, we first derived the q-NSCH system for MCLs with variable density by using energy variational method consistently. GNBC for mass-averaged velocity is obtained during the variation due to the boundary dissipation.

Then based on previous work [51], we designed an energy stable C^0 finite element scheme to solve the obtained q-NSCH system with slip boundary condition. We also proved that the fully discrete scheme is mass conservative for each phase. Thanks to the quasi-incompressible condition with Δp term, the finite element space for Navier-Stokes equations do not need to satisfy the Babuska-Brezzi inf-sup condition, as in the case of the pressure stabilization method for the standard Navier-Stokes equations.

Three examples are investigated numerically. The Couette flow test illustrates the 2nd-order for P^1 element and 3rd-order for P^2 element convergence rate in the sense of L^2 norm and the energy decay of the scheme. The contact angle effect on the droplet is illustrated by moving droplet in shear flow. Finally, a rising bubble is simulated to confirm the ability of our scheme to handle large density ratio and the quasi-incompressibility only happens around the interface.

Authors' contributions

L.S, Z.S, and S.X did the model derivations. L.S, P.L and S.X carried out the numerical analysis and simulations. H.H and P.L designed the study. H.H, P.L and S.X coordinated the study. All participated on the preparation of the manuscript. All authors gave final approval for publication.

Declaration of competing interest

The authors declare that they have no known competing financial interests or personal relationships that could have appeared to influence the work reported in this paper.

Acknowledgements

This work was partially supported by the NSFC (grant numbers 11771040, 11861131004, 91430106), NSERC (CA) and the Fields Institute. Lingyue Shen was partially supported by the Chinese Scholarship Council for studying at the University of Dundee.

Appendix A. Energy variation details

For the first term I_1 in (16), using the last two equations in Eq. (8) yields

$$\begin{aligned}
 I_1 &= \frac{d}{dt} \int_{\Omega} \frac{\rho |\mathbf{u}|^2}{2} d\mathbf{x} \\
 &= \int_{\Omega} \frac{1}{2} \frac{\partial \rho}{\partial t} |\mathbf{u}|^2 d\mathbf{x} + \int_{\Omega} \rho \frac{\partial \mathbf{u}}{\partial t} \cdot \mathbf{u} d\mathbf{x} \\
 &= \int_{\Omega} \frac{1}{2} \frac{\partial \rho}{\partial t} |\mathbf{u}|^2 d\mathbf{x} + \int_{\Omega} \rho \frac{D\mathbf{u}}{Dt} \cdot \mathbf{u} d\mathbf{x} - \int_{\Omega} (\rho \mathbf{u} \cdot \nabla \mathbf{u}) \cdot \mathbf{u} d\mathbf{x}
 \end{aligned}$$

$$\begin{aligned}
&= \int_{\Omega} \frac{1}{2} \frac{\partial \rho}{\partial t} |\mathbf{u}|^2 d\mathbf{x} + \int_{\Omega} \rho \frac{D\mathbf{u}}{Dt} \cdot \mathbf{u} d\mathbf{x} + \int_{\Omega} \nabla \cdot (\rho \mathbf{u}) \frac{|\mathbf{u}|^2}{2} d\mathbf{x} \\
&= \int_{\Omega} (\nabla \cdot (\boldsymbol{\sigma}_{\eta} + \boldsymbol{\sigma}_c)) \cdot \mathbf{u} d\mathbf{x} + \int_{\Omega} p \left(\frac{1}{\rho^2} \frac{d\rho}{dc} \nabla \cdot \mathbf{j}_c - \nabla \cdot \mathbf{u} \right) d\mathbf{x} \\
&= \int_{\Omega} (\nabla \cdot (\boldsymbol{\sigma}_{\eta} + \boldsymbol{\sigma}_c)) \cdot \mathbf{u} d\mathbf{x} + \int_{\Omega} p (-\alpha \nabla \cdot \mathbf{j}_c - \nabla \cdot \mathbf{u}) d\mathbf{x} \\
&= - \int_{\Omega} (\boldsymbol{\sigma}_{\eta} : \nabla \mathbf{u} + \boldsymbol{\sigma}_c : \nabla \mathbf{u}) d\mathbf{x} + \int_{\Omega} \nabla(\alpha p) \cdot \mathbf{j}_c d\mathbf{x} - \int_{\Omega} p \nabla \cdot \mathbf{u} d\mathbf{x} \\
&\quad + \int_{\partial\Omega_w} ((\boldsymbol{\sigma}_{\eta} + \boldsymbol{\sigma}_c) \cdot \mathbf{n}) \cdot \mathbf{u}_{\tau} dS, \tag{A.1}
\end{aligned}$$

where we have introduced a Lagrangian multiplier p with respect to the constraint (11) and have used the boundary condition $\mathbf{u} \cdot \mathbf{n} = 0$ and $\mathbf{j}_c \cdot \mathbf{n} = 0$.

For the second term I_2 in (16), using the first equation in Eq. (8) and last two boundary conditions in Eq. (12) yields

$$\begin{aligned}
I_2 &= \frac{d}{dt} \int_{\Omega} \rho \lambda_c \left(G(c) + \frac{\gamma^2}{2} |\nabla c|^2 \right) d\mathbf{x} \\
&= \int_{\Omega} \rho \lambda_c \frac{D}{Dt} \left(G + \frac{\gamma^2}{2} |\nabla c|^2 \right) d\mathbf{x} \\
&= \int_{\Omega} \rho \lambda_c \frac{dG}{dc} \frac{Dc}{Dt} d\mathbf{x} + \int_{\Omega} \rho \lambda_c \gamma^2 \left(\nabla c \cdot \frac{D}{Dt} (\nabla c) \right) d\mathbf{x} \\
&= \int_{\Omega} \rho \lambda_c \frac{dG}{dc} \frac{Dc}{Dt} d\mathbf{x} + \int_{\Omega} \rho \lambda_c \gamma^2 \left(\nabla c \cdot \left(\frac{\partial}{\partial t} (\nabla c) + (\mathbf{u} \cdot \nabla) (\nabla c) \right) \right) d\mathbf{x} \\
&= \int_{\Omega} \rho \lambda_c \frac{dG}{dc} \frac{Dc}{Dt} d\mathbf{x} + \int_{\Omega} \rho \lambda_c \gamma^2 \left(\nabla c \cdot \left(\nabla \frac{\partial c}{\partial t} \right) \right) d\mathbf{x} + \int_{\Omega} \rho \lambda_c \gamma^2 (\partial_i c u_j \partial_j^2 c) d\mathbf{x} \\
&= \int_{\Omega} \rho \lambda_c \frac{dG}{dc} \frac{Dc}{Dt} d\mathbf{x} + \int_{\Omega} \rho \lambda_c \gamma^2 \left(\nabla c \cdot \left(\nabla \frac{\partial c}{\partial t} \right) \right) d\mathbf{x} \\
&\quad + \int_{\Omega} \rho \lambda_c \gamma^2 (\partial_i c \partial_i (u_j \partial_j c) - \partial_i c \partial_j c \partial_i u_j) d\mathbf{x} \\
&= \int_{\Omega} \rho \lambda_c \frac{dG}{dc} \frac{Dc}{Dt} d\mathbf{x} + \int_{\Omega} \rho \lambda_c \gamma^2 \nabla c \cdot \nabla \left(\frac{Dc}{Dt} \right) d\mathbf{x} - \int_{\Omega} \rho \lambda_c \gamma^2 (\nabla c \otimes \nabla c) : \nabla \mathbf{u} d\mathbf{x} \\
&= \int_{\Omega} \rho \lambda_c \frac{dG}{dc} \frac{Dc}{Dt} d\mathbf{x} - \int_{\Omega} \nabla \cdot \left(\rho \lambda_c \gamma^2 \nabla c \right) \left(\frac{Dc}{Dt} \right) d\mathbf{x} - \int_{\Omega} \rho \lambda_c \gamma^2 (\nabla c \otimes \nabla c) : \nabla \mathbf{u} d\mathbf{x} \\
&\quad + \int_{\partial\Omega_w} \rho \lambda_c \gamma^2 \partial_n c \frac{D_{\Gamma} c}{Dt} dS \\
&= \int_{\Omega} \rho \mu \frac{Dc}{Dt} d\mathbf{x} - \int_{\Omega} \lambda_c \gamma^2 (\rho \nabla c \otimes \nabla c) : \nabla \mathbf{u} d\mathbf{x} + \int_{\partial\Omega_w} \rho \lambda_c \gamma^2 \partial_n c \frac{D_{\Gamma} c}{Dt} dS \\
&= - \int_{\Omega} \mu \nabla \cdot \mathbf{j}_c d\mathbf{x} - \int_{\Omega} \lambda_c \gamma^2 (\rho \nabla c \otimes \nabla c) : \nabla \mathbf{u} d\mathbf{x} + \int_{\partial\Omega_w} \rho \lambda_c \gamma^2 \partial_n c \frac{D_{\Gamma} c}{Dt} dS \\
&= \int_{\Omega} \nabla \mu \cdot \mathbf{j}_c d\mathbf{x} - \int_{\Omega} \lambda_c \gamma^2 (\rho \nabla c \otimes \nabla c) : \nabla \mathbf{u} d\mathbf{x} + \int_{\partial\Omega_w} \rho \lambda_c \gamma^2 \partial_n c \frac{D_{\Gamma} c}{Dt} dS
\end{aligned}$$

(A.2)

where $\mu = \lambda_c \left(\frac{dG}{dc} - \frac{1}{\rho} \gamma^2 \nabla \cdot (\rho \nabla c) \right)$.

Appendix B. Proof of Lemma 2.1

Proof.

$$\begin{aligned}
 & \frac{d}{dt} \int_{\Omega} (\rho(\mathbf{x}, t) f(\mathbf{x}, t)) d\mathbf{x} \\
 &= \int_{\Omega} \frac{\partial \rho}{\partial t} f + \rho \frac{\partial f}{\partial t} d\mathbf{x} \\
 &= - \int_{\Omega} \nabla \cdot (\mathbf{u} \rho) f d\mathbf{x} + \int_{\Omega} \rho \frac{\partial f}{\partial t} d\mathbf{x} \\
 &= \int_{\Omega} \rho \left(\frac{\partial f}{\partial t} + \mathbf{u} \cdot \nabla f \right) d\mathbf{x} \\
 &= \int_{\Omega} \rho \frac{Df}{Dt} d\mathbf{x}. \quad \square
 \end{aligned} \tag{B.1}$$

Appendix C. Tensor calculation

$$\begin{aligned}
 & (\nabla \mathbf{u} + (\nabla \mathbf{u})^T) : \nabla \mathbf{u} - \frac{2}{3} (\nabla \cdot \mathbf{u})^2 \\
 &= \sum_{i,j=1,2,3} (\partial_i u_j + \partial_j u_i) \partial_j u_i - \frac{2}{3} \sum_{i=1,2,3} (\partial_i u_i)^2 \\
 &= \sum_{i=1,2,3} 2(\partial_i u_i)^2 + \sum_{i<j} 2(\partial_i u_j + \partial_j u_i) \partial_j u_i - \frac{2}{3} \sum_{i=1,2,3} (\partial_i u_i)^2 - \frac{2}{3} \sum_{i<j} 2(\partial_i u_i \partial_j u_j) \\
 &= \sum_{i<j} (\partial_i u_j + \partial_j u_i)^2 + \frac{4}{3} \left(\sum_{i=1,2,3} (\partial_i u_i)^2 - \sum_{i<j} (\partial_i u_i \partial_j u_j) \right) \\
 &= \sum_{i<j} (\partial_i u_j + \partial_j u_i)^2 + \frac{2}{3} \sum_{i<j} (\partial_i u_i - \partial_j u_j)^2
 \end{aligned} \tag{C.1}$$

References

- [1] E.B. Dussan V., S.H. Davis, On the motion of a fluid-fluid interface along a solid surface, *J. Fluid Mech.* 65 (1) (1974) 71–95, <https://doi.org/10.1017/S0022112074001261>.
- [2] E.B. Dussan, On the spreading of liquids on solid surfaces: static and dynamic contact lines, *Annu. Rev. Fluid Mech.* 11 (1) (1979) 371–400, <https://doi.org/10.1146/annurev.fl.11.010179.002103>.
- [3] S. Kumar, Liquid transfer in printing processes: liquid bridges with moving contact lines, *Annu. Rev. Fluid Mech.* 47 (1) (2015) 67–94, <https://doi.org/10.1146/annurev-fluid-010814-014620>.
- [4] J. Breitenbach, I.V. Roisman, C. Tropea, From drop impact physics to spray cooling models: a critical review, *Exp. Fluids* 59 (3) (2018) 55, <https://doi.org/10.1007/s00348-018-2514-3>.
- [5] S. Xu, Z. Xu, O.V. Kim, R.I. Litvinov, J.W. Weisel, M. Alber, Model predictions of deformation, embolization and permeability of partially obstructive blood clots under variable shear flow, *J. R. Soc. Interface* 14 (136) (2017), <https://doi.org/10.1098/rsif.2017.0441>.
- [6] C.-k. Tung, O. Krupa, E. Apaydin, J.-J. Liou, A. Diaz-Santana, B. Jun Kim, M. Wu, A contact line pinning based microfluidic platform for modelling physiological flows, *Lab Chip* 13 (19) (2013) 3876–3885, <https://doi.org/10.1039/C3LC50489A>.
- [7] J.-J. Xu, W. Ren, A level-set method for two-phase flows with moving contact line and insoluble surfactant, *J. Comput. Phys.* 263 (2014) 71–90.
- [8] Z. Zhang, S. Xu, W. Ren, Derivation of a continuum model and the energy law for moving contact lines with insoluble surfactants, *Phys. Fluids* 26 (6) (2014) 062103, <https://doi.org/10.1063/1.4881195>.
- [9] J. Koplik, J.R. Banavar, J.F. Willemsen, Molecular dynamics of Poiseuille flow and moving contact lines, *Phys. Rev. Lett.* 60 (13) (1988) 1282–1285, <https://doi.org/10.1103/PhysRevLett.60.1282>.
- [10] J. Koplik, J.R. Banavar, J.F. Willemsen, Molecular dynamics of fluid flow at solid surfaces, *Phys. Fluids A* 1 (1989) 15.
- [11] E.R. Smith, P.E. Theodorakis, R.V. Craster, O.K. Matar, Moving contact lines: linking molecular dynamics and continuum-scale modeling, *Langmuir* 34 (42) (2018) 12501–12518, <https://doi.org/10.1021/acs.langmuir.8b00466>.

- [12] K. Bao, Y. Shi, S. Sun, X.-P. Wang, A finite element method for the numerical solution of the coupled Cahn–Hilliard and Navier–Stokes system for moving contact line problems, *J. Comput. Phys.* 231 (24) (2012) 8083–8099.
- [13] Y. Jiang, P. Lin, Z. Guo, S. Dong, Numerical simulation for moving contact line with continuous finite element schemes, *Commun. Comput. Phys.* 18 (1) (2015) 180–202, <https://doi.org/10.4208/cicp.170314.160115a>.
- [14] T. Qian, X.-P. Wang, P. Sheng, A variational approach to moving contact line hydrodynamics, *J. Fluid Mech.* 564 (2006) 333, <https://doi.org/10.1017/S0022112006001935>.
- [15] T. Qian, X.-P. Wang, P. Sheng, Molecular hydrodynamics of the moving contact line in two-phase immiscible flows, *Commun. Comput. Phys.* (2006) 52.
- [16] A.J. Salgado, A diffuse interface fractional time-stepping technique for incompressible two-phase flows with moving contact lines, *ESAIM: Math. Model. Numer. Anal.* 47 (3) (2013) 743–769, <https://doi.org/10.1051/m2an/2012047>.
- [17] J. Shen, X. Yang, H. Yu, Efficient energy stable numerical schemes for a phase field moving contact line model, *J. Comput. Phys.* 284 (2015) 617–630, <https://doi.org/10.1016/j.jcp.2014.12.046>.
- [18] L. Ma, R. Chen, X. Yang, H. Zhang, Numerical approximations for Allen–Cahn type phase field model of two-phase incompressible fluids with moving contact lines, *Commun. Comput. Phys.* 21 (3) (2017) 867–889.
- [19] A.E. Diegel, S.W. Walker, A finite element method for a phase field model of nematic liquid crystal droplets, *Commun. Comput. Phys.* 25 (2019) 155–188.
- [20] N.G. Hadjicostantinou, Hybrid atomistic-continuum formulations and the moving contact line problem, *J. Comput. Phys.* 154 (2) (1999) 245–265, <https://doi.org/10.1006/jcph.1999.6302>.
- [21] W. Ren, W. E, Heterogeneous multiscale method for the modeling of complex fluids and micro-fluidics, *J. Comput. Phys.* 204 (1) (2005) 1–26, <https://doi.org/10.1016/j.jcp.2004.10.001>.
- [22] M.-C. Lai, Y.-H. Tseng, H. Huang, Numerical simulation of moving contact lines with surfactant by immersed boundary method, *Commun. Comput. Phys.* (2010), <https://doi.org/10.4208/cicp.281009.120210a>.
- [23] W. Ren, W. E, Boundary conditions for the moving contact line problem, *Phys. Fluids* 19 (2) (2007) 022101.
- [24] W. Ren, D. Hu, W. E, Continuum models for the contact line problem, *Phys. Fluids* 22 (10) (2010) 102103.
- [25] J. Huang, X.-P. Wang, A lattice Boltzmann model for multiphase flows with moving contact line and variable density, *J. Comput. Phys.* 353 (2018) 26–45.
- [26] T. Lu, A mass conservative lattice Boltzmann model for two-phase flows with moving contact lines at high density ratio, *Commun. Comput. Phys.* 26 (2019) 1098–1117.
- [27] D. Bonn, J. Eggers, J. Indekeu, J. Meunier, E. Rolley, Wetting and spreading, *Rev. Mod. Phys.* 81 (2) (2009) 739–805, <https://doi.org/10.1103/RevModPhys.81.739>.
- [28] J.H. Snoeijer, B. Andreotti, Moving contact lines: scales, regimes, and dynamical transitions, *Annu. Rev. Fluid Mech.* 45 (1) (2013) 269–292, <https://doi.org/10.1146/annurev-fluid-011212-140734>.
- [29] D.M. Anderson, G.B. McFadden, A.A. Wheeler, Diffuse-interface methods in fluid mechanics, *Annu. Rev. Fluid Mech.* 30 (1998) 139–165, <https://doi.org/10.1146/annurev.fluid.30.1.139>.
- [30] M.E. Gurtin, D. Polignone, J. Viñals, Two-phase binary fluids and immiscible fluids described by an order parameter, *Math. Models Methods Appl. Sci.* 6 (6) (1996) 815–831, <https://doi.org/10.1142/S0218202596000341>.
- [31] D. Jacqmin, Calculation of two-phase Navier–Stokes flows using phase-field modeling, *J. Comput. Phys.* 155 (1) (1999) 96–127, <https://doi.org/10.1006/jcph.1999.6332>.
- [32] K. Cheng, C. Wang, S.M. Wise, X. Yue, A second-order, weakly energy-stable pseudo-spectral scheme for the Cahn–Hilliard equation and its solution by the homogeneous linear iteration method, *J. Sci. Comput.* 69 (3) (2016) 1083–1114.
- [33] J. Guo, C. Wang, S.M. Wise, X. Yue, An H^2 convergence of a second-order convex-splitting, finite difference scheme for the three-dimensional Cahn–Hilliard equation, *Commun. Math. Sci.* 14 (2) (2016) 489–515.
- [34] Y. Yan, W. Chen, C. Wang, S.M. Wise, A second-order energy stable BDF numerical scheme for the Cahn–Hilliard equation, *Commun. Comput. Phys.* 23 (2) (2018) 572–602.
- [35] Q. Du, C. Liu, X. Wang, Retrieving topological information for phase field models, *SIAM J. Appl. Math.* 65 (2005) 1913–1932.
- [36] J.J. Feng, C. Liu, J. Shen, P. Yue, An energetic variational formulation with phase field methods for interfacial dynamics of complex fluids: advantages and challenges, in: *Modeling of Soft Matter*, 2005, pp. 1–26, https://doi.org/10.1007/0-387-32153-5_1.
- [37] P. Yue, J.J. Feng, C. Liu, J. Shen, A diffuse-interface method for simulating two-phase flows of complex fluids, *J. Fluid Mech.* 515 (2004) 293–317, <https://doi.org/10.1017/S0022112004000370>.
- [38] C. Liu, J. Shen, X. Yang, Decoupled energy stable schemes for a phase-field model of two-phase incompressible flows with variable density, *J. Sci. Comput.* 62 (2) (2015) 601–622, <https://doi.org/10.1007/s10915-014-9867-4>.
- [39] K. Cheng, W. Feng, C. Wang, S.M. Wise, An energy stable fourth order finite difference scheme for the Cahn–Hilliard equation, *J. Comput. Appl. Math.* 362 (2019) 574–595.
- [40] A.E. Diegel, C. Wang, S.M. Wise, Stability and convergence of a second-order mixed finite element method for the Cahn–Hilliard equation, *IMA J. Numer. Anal.* 36 (4) (2015) 1867–1897.
- [41] J. Shen, X. Yang, Energy stable schemes for Cahn–Hilliard phase-field model of two-phase incompressible flows, *Chin. Ann. Math., Ser. B* 31 (5) (2010) 743–758, <https://doi.org/10.1007/s11401-010-0599-y>.
- [42] J. Shen, X. Yang, Decoupled energy stable schemes for phase-field models of two-phase incompressible flows, *SIAM J. Numer. Anal.* 53 (1) (2015) 279–296, <https://doi.org/10.1137/140971154>.
- [43] C. Liu, J. Shen, A phase field model for the mixture of two incompressible fluids and its approximation by a Fourier-spectral method, *Physica D: Nonlin. Phenom.* 179 (3–4) (2003) 211–228.
- [44] J. Lowengrub, L. Truskinovsky, Quasi-incompressible Cahn–Hilliard fluids and topological transitions, *Proc. R. Soc., Math. Phys. Eng. Sci.* 454 (1978) (1998) 2617–2654, <https://doi.org/10.1098/rspa.1998.0273>.
- [45] J. Shen, X. Yang, Q. Wang, Mass and volume conservation in phase field models for binary fluids, *Commun. Comput. Phys.* 13 (4) (2013) 1045–1065, <https://doi.org/10.4208/cicp.300711.160212a>.
- [46] H. Abels, H. Garcke, G. Grün, Thermodynamically consistent diffuse interface models for incompressible two-phase flows with different densities, *arXiv:1011.0528*, Nov. 2010.
- [47] F. Boyer, Nonhomogeneous Cahn–Hilliard fluids, *Ann. Inst. Henri Poincaré, Anal. Non Linéaire* 18 (2) (2001) 225–259, [https://doi.org/10.1016/S0294-1449\(00\)00063-9](https://doi.org/10.1016/S0294-1449(00)00063-9).
- [48] H. Ding, P.D. Spelt, C. Shu, Diffuse interface model for incompressible two-phase flows with large density ratios, *J. Comput. Phys.* 226 (2) (2007) 2078–2095, <https://doi.org/10.1016/j.jcp.2007.06.028>.
- [49] J. Shen, X. Yang, A phase-field model and its numerical approximation for two-phase incompressible flows with different densities and viscosities, *SIAM J. Sci. Comput.* 32 (3) (2010) 1159–1179, <https://doi.org/10.1137/09075860X>.
- [50] H. Abels, H. Garcke, G. Grün, Thermodynamically consistent, frame indifferent diffuse interface models for incompressible two-phase flows with different densities, *Math. Models Methods Appl. Sci.* 22 (3) (2012) 1150013, <https://doi.org/10.1142/S0218202511500138>.

- [51] Z. Guo, P. Lin, J. Lowengrub, S.M. Wise, Mass conservative and energy stable finite difference methods for the quasi-incompressible Navier-Stokes-Cahn-Hilliard system: primitive variable and projection-type schemes, *Comput. Methods Appl. Mech. Eng.* 326 (2017) 144–174, <https://doi.org/10.1016/j.cma.2017.08.011>.
- [52] B. Eisenberg, Y. Hyon, C. Liu, Energy variational analysis of ions in water and channels: field theory for primitive models of complex ionic fluids, *J. Chem. Phys.* 133 (10) (2010) 104104.
- [53] C. Liu, H. Wu, An energetic variational approach for the Cahn–Hilliard equation with dynamic boundary condition: model derivation and mathematical analysis, *Arch. Ration. Mech. Anal.* (2019) 1–81.
- [54] S. Xu, B. Eisenberg, Z. Song, H. Huang, Osmosis through a semi-permeable membrane: a consistent approach to interactions, preprint, arXiv:1806.00646, 2018.
- [55] M. Gao, X.-P. Wang, A gradient stable scheme for a phase field model for the moving contact line problem, *J. Comput. Phys.* 231 (4) (2012) 1372–1386, <https://doi.org/10.1016/j.jcp.2011.10.015>.
- [56] M. Gao, X.-P. Wang, An efficient scheme for a phase field model for the moving contact line problem with variable density and viscosity, *J. Comput. Phys.* 272 (2014) 704–718, <https://doi.org/10.1016/j.jcp.2014.04.054>.
- [57] S. Xu, M. Alber, Z. Xu, Three-phase model of visco-elastic incompressible fluid flow and its computational implementation, *Commun. Comput. Phys.* 25 (2) (2019) 586–624.
- [58] H. Yu, X. Yang, Numerical approximations for a phase-field moving contact line model with variable densities and viscosities, *J. Comput. Phys.* 334 (2017) 665–686, <https://doi.org/10.1016/j.jcp.2017.01.026>.
- [59] L. Luo, X.-P. Wang, X.-C. Cai, An efficient finite element method for simulation of droplet spreading on a topologically rough surface, *J. Comput. Phys.* 349 (2017) 233–252.
- [60] Q. Zhang, T.-Z. Qian, X.-P. Wang, Phase field simulation of a droplet impacting a solid surface, *Phys. Fluids* 28 (2) (2016) 022103.
- [61] S. Dong, J. Shen, A time-stepping scheme involving constant coefficient matrices for phase-field simulations of two-phase incompressible flows with large density ratios, *J. Comput. Phys.* 231 (17) (2012) 5788–5804, <https://doi.org/10.1016/j.jcp.2012.04.041>.
- [62] X. Yang, H. Yu, Efficient second order unconditionally stable schemes for a phase field moving contact line model using an invariant energy quadratization approach, *SIAM J. Sci. Comput.* 40 (3) (2018) B889–B914.
- [63] A.E. Diegel, C. Wang, X. Wang, S.M. Wise, Convergence analysis and error estimates for a second order accurate finite element method for the Cahn–Hilliard–Navier–Stokes system, *Numer. Math.* 137 (3) (2017) 495–534.
- [64] Y. Liu, W. Chen, C. Wang, S.M. Wise, Error analysis of a mixed finite element method for a Cahn–Hilliard–Hele–Shaw system, *Numer. Math.* 135 (3) (2017) 679–709.
- [65] Z. Guo, P. Lin, J.S. Lowengrub, A numerical method for the quasi-incompressible Cahn–Hilliard–Navier–Stokes equations for variable density flows with a discrete energy law, *J. Comput. Phys.* 276 (2014) 486–507.
- [66] F. Brezzi, J. Pitkäranta, On the stabilization of finite element approximations of the Stokes equations, in: *Efficient Solutions of Elliptic Systems*, 1984, pp. 11–19.
- [67] R. Rannacher, On the numerical solution of the incompressible Navier–Stokes equations, *Z. Angew. Math. Mech.* 73 (9) (1993) 203–216.
- [68] J. Shen, On pressure stabilization method and projection method for unsteady Navier–Stokes equations, in: *Advances in Computer Methods for Partial Differential Equations*, 1992, pp. 658–662.
- [69] P. Lin, A sequential regularization method for time-dependent incompressible Navier–Stokes equations, *SIAM J. Numer. Anal.* 34 (3) (1997) 1051–1071.
- [70] P. Lin, X. Chen, M.T. Ong, Finite element methods based on a new formulation for the non-stationary incompressible Navier–Stokes equations, *Int. J. Numer. Methods Fluids* 46 (12) (2004) 1169–1180.
- [71] P. Lin, C. Liu, Simulations of singularity dynamics in liquid crystal flows: a C^0 finite element approach, *J. Comput. Phys.* 215 (1) (2006) 348–362.
- [72] Z. Guo, P. Lin, A thermodynamically consistent phase-field model for two-phase flows with thermocapillary effects, *J. Fluid Mech.* 766 (2015) 226–271.
- [73] S. Xu, P. Sheng, C. Liu, An energetic variational approach for ion transport, *Commun. Math. Sci.* 12 (4) (2014) 779–789.
- [74] J. Shen, J. Xu, J. Yang, The scalar auxiliary variable (SAV) approach for gradient flows, *J. Comput. Phys.* 353 (2018) 407–416.
- [75] Y. Gong, J. Zhao, Q. Wang, Arbitrarily high-order unconditionally energy stable SAV schemes for gradient flow models, *Comput. Phys. Commun.* (2019) 107033.
- [76] D.J. Eyre, Unconditionally gradient stable time marching the Cahn–Hilliard equation, *MRS Online Proc. Libr. Arch.* 529 (1998).
- [77] S.M. Wise, C. Wang, J.S. Lowengrub, An energy-stable and convergent finite-difference scheme for the phase field crystal equation, *SIAM J. Numer. Anal.* 47 (3) (2009) 2269–2288.
- [78] Z. Hu, S.M. Wise, C. Wang, J.S. Lowengrub, Stable and efficient finite-difference nonlinear-multigrid schemes for the phase field crystal equation, *J. Comput. Phys.* 228 (15) (2009) 5323–5339.
- [79] F. Hecht, New development in FreeFem++, *J. Numer. Math.* 20 (3–4) (2012) 251–265.